Reduction of nucleolar NOC1 accumulates pre-rRNAs and induces Xrp1 affecting growth and resulting in cell competition

Francesca Destefanis[1,*], Valeria Manara[1,*], Stefania Santarelli[1,*], Sheri Zola[1], Marco Brambilla[2], Giacomo Viola[2], Paola Maragno[1], Ilaria Signoria[3], Gabriella Viero[3], Maria Enrica Pasini[2], Marianna Penzo[5,6], and Paola Bellosta[1,2,4,‡]

[1]Department of Cellular, Computational and Integrative Biology (CIBIO), University of Trento, Via Sommarive 9, 38123 Trento, Italy
[2]Department of Biosciences, University of Milano, Via Celoria 25, 20133 Milano, Italy
[3]Institute of Biophysics, CNR, Via Sommarive 18, 38123 Trento, Italy
[4]Department of Medicine NYU Langone School of Medicine, 550 First Avenue, 10016, NY, USA
[5]Department of Experimental, Diagnostic and Specialty Medicine, University of Bologna, Via Massarenti 9, 40138 Bologna, Italy
[6]Center for Applied Biomedical Research, University of Bologna, Via Massarenti 9, 40138 Bologna, Italy

*equally contributed
‡corresponding author: paola.bellosta@unitn.it

summary statement

NOC1 is a nucleolar protein necessary for rRNA maturation and protein synthesis. Its reduction results in apoptosis and cell competition accompanied by upregulation of Xrp1 and of DILP8

Abstract

NOC1 is a nucleolar protein necessary in yeast for both transport and maturation of ribosomal subunits. Here, we show that *Drosophila* NOC1 is necessary for rRNAs maturation and for a correct animal development. Its ubiquitous downregulation results in a dramatic decrease in polysome level and of protein synthesis. NOC1 expression in multiple organs, such as the prothoracic gland and the fat body, is necessary for their proper functioning. Reduction of NOC1 in epithelial cells from the imaginal discs results in clones that die by apoptosis, an event that is partially rescued in a *M/+* background, suggesting that reduction of NOC1 induces the cells

to become less fitted and to acquire a loser state. NOC1 downregulation activates the pro-apoptotic eiger-JNK pathway and leads to an increase of Xrp1 that results in Dilp8 upregulation. These data underline NOC1 as an essential gene in ribosome biogenesis and highlight its novel functions in the control of growth and cell competition.

Keywords: Drosophila, NOC1, eiger, DILP8, Xrp1, cell competition, apoptosis.

Introduction

NOC1, 2 and 3 are members of a large family of conserved nucleolar proteins that play a critical role in the control of ribosome biogenesis in yeast and plants (Edskes et al., 1998; Li et al., 2009). Studies in *S. cerevisiae* reveal that NOCs proteins are required for the maturation and processing of the rRNAs (Khoshnevis et al., 2019) and for transport of the pre-ribosomal 60S subunit in the cytoplasm through the formation of NOC1/NOC2 and NOC2/NOC3 heterodimers (Hierlmeier et al., 2013; Milkereit et al., 2001). NOC1-3 function is unique and essential, as mutation in each gene affects growth and viability in both *S. cerevisiae* and in *Arabidopsis* (Edskes et al., 1998; Li et al., 2009; Milkereit et al., 2001).

In *Drosophila,* efficient ribosome biogenesis is necessary during larval development, when increase in cell mass and animal size is highly dependent on protein synthesis (Texada et al., 2020). Mutations in genes that regulate this process, like those encoding for *Minute* ribosomal proteins (Marygold et al., 2007; Saeboe-Larssen et al., 1998) or for *Nop60b/Dyskerin* (Tortoriello et al., 2010) and *Nopp140* (Baral et al., 2020), components of the nucleolus, present common defects that include a delay in development and reduced body size. Similar phenotypes have also been described for mutations in genes that control rRNA synthesis, such as the RNA-Pol-I associated chromatin regulator *PWP1* (Liu et al., 2017) or the *Rpl-135* subunit of the Pol-I complex (Grewal et al., 2005), and for *diminutive* (*dm*), the gene encoding for MYC (Johnston et al., 1999), a master regulator of ribosome biogenesis both in *Drosophila* and in vertebrates (Barna et al., 2008; Destefanis et al., 2020; Grewal et al., 2005; van Riggelen et al., 2010).

Larval growth is also regulated by *Drosophila* insulin-like peptides DILPs (DILP2, 3 and 5) released from the Insulin Producing Cells (IPCs) in response to nutrients (Geminard et al., 2009; Koyama et al., 2020; Maniere et al., 2020). This process is

developmentally coordinated by the growth hormone ecdysone, secreted by the ring gland (Nijhout et al., 2014), and indirectly by DILP8, a peptide member of the Insulin/Relaxin family, secreted by cells from the peripheral organs in response to tissue damage (Garelli et al., 2015; Vallejo et al., 2015). The release of DILP8 blocks ecdysone synthesis and delays development to ensure proper regeneration of the damaged organ with developmental timing (Boulan and Leopold, 2021). In cells of the imaginal discs, DILP8 upregulation has been associated with cell damage induced by the activation of eiger/JNK pathway (Sanchez et al., 2019), and more recently with the transcriptional upregulation of the Xrp1-RpS12 axis (Boulan and Leopold, 2021) that links signals of inter-organ coordination with proteotoxic stress. Indeed, reduced protein synthesis activates a stress response which triggers the activation of Xrp1, a pro-apoptotic CCAAT-Enhancer-Binding Protein (C/EBP) transcription factor that by reducing translation activates the elimination of the unfitted cells by cell competition (Baillon et al., 2018; Brown et al., 2021; Kiparaki et al., 2022; Langton et al., 2021). Mutations in ribosomal proteins, such as RpS3 (Akai et al., 2021; Baumgartner et al., 2021) and RpS12 (Ji et al., 2019; Lee et al., 2018), and the activation of the JNK/STAT signaling pathway (Kucinski et al., 2017), have been shown to control proteotoxic-induced cell competition revealing how this process may by regulated by a complex network of signaling.

In this study we characterized the function of *Drosophila* nucleolar NOC1, NOC2 and NOC3 *in vivo* and showed that their expression is necessary for proper animal growth. We demonstrated that NOC1 controls polysome abundance and its ubiquitous reduction blocks rRNA maturation resulting in reduced protein synthesis. In line with these results, lowering NOC1 levels in the whole animal results in small larvae that die early during development, while its reduction in different organs causes specific impairments of their function. In cells of the wing imaginal disc, NOC1 downregulation induces apoptosis that is partially rescued in a *Minute*/+ background and by the expression of the caspase inhibitor P35, a behavior that was typically described in loser cells and for genes that control cell competition. Our data identify that NOC1-RNAi cells show Xrp1 upregulation as well as activation of eiger and JNK pathways, followed by an increase of DILP8 expression. However, DILP8 upregulation in our model is independent of eiger expression, suggesting that Xrp1 may be inducing apoptosis in NOC1-RNAi by controlling specific pathways driven by proteotoxic stress.

Results

Drosophila NOC1 localizes in the nucleolus and is necessary for animal growth

NOCs (Nucleolar complex associated) are members of a protein family characterized by the presence of a NOC domain, not conserved in all proteins, and necessary for their heterodimerization (Milkereit et al., 2001). In *Drosophila,* the orthologues of yeast *Noc1*, *Noc2* and *Noc3* are annotated as *CG7839, CG9246* and *CG1234,* and are hereinafter called *NOC1, NOC2 and NOC3.* These genes, present also in humans, have a grade of conservation that varies from 32% to 35% of homology within their amino acid sequences (Figure 1A). Interestingly, a network analysis using the STRING database on predicted protein-protein interactions for NOC1/CG7839 uncovers that all three NOC proteins form a hub with other nucleolar proteins with a distinct role in ribosome biogenesis, suggesting that NOCs may function in concert to ensure proper nucleolar activity (Supplementary Figure 1).

Our results showed that ubiquitous reduction of NOC1, 2 or 3 in *Drosophila*, using RNAi interference in combination with the *actin* promoter resulted in small larvae that died between first and second instar (Figure 1B, Table 1 and Supplementary Figure 2A). Similar results were obtained by CRISPR-Cas9 mediated homozygous mutation of *NOC1* (Figure 1C, and Supplementary Figure 3). On the contrary, overexpression of NOC1 led to larvae that reached pupariation at almost the same size as the control but failed to maturate into adult animals. These data suggest that NOC1 is fundamental, and its expression must be tightly controlled to ensure proper animal development. These conclusions support the experiments which demonstrated that the coexpression of NOC1 compensates for NOC1 reduction allowing larvae to develop (Figure 1D, E) and to mature into small but viable adults (Figure 1F, G-H). NOC1 function is unique indeed it does not complement for NOC2 or NOC3 reduction since co-expression of NOC1 failed to rescue the lethality of NOC2-RNAi and NOC3-RNAi animals (not shown). Next, we used the line CG7839-GFP.FPTB, (modENCODE Model Organism ENCyclopedia Of DNA regulatory Elements), in which GFP-CG7839/NOC1 is expressed under the control of its regulatory sequences (Kudron et al., 2018) and showed that NOC1-GFP is expressed primarily in the nucleolus and colocalizing with fibrillarin in cells of the wing imaginal discs (Figure 1I). The same result was confirmed in cells of the salivary glands where the nucleolus is more evident (data not shown). Since no commercial antibodies are

available to characterize the endogenous protein, we expressed an HA- tagged form of NOC1 and determined its molecular weight as 132 KDa in lysates from 3rd instar larvae. In addition, we observed the presence of multiple bands at lower molecular weights detected with anti HA antibodies (Figure 1J), suggesting that NOC1 may undergo to unusual proteolytic processes that may be linked to its toxicity observed in larvae at pupae transition (Table1). Overexpression of HA-NOC1 in the columnar epithelium of the wing imaginal discs using the *engrailed* promoter confirmed its colocalization with fibrillarin in the nucleolus (Figure 1K-K'), this observation was better defined using the large cells of peripodium (Figure 1M-M'). In addition, we noticed that when overexpressed NOC1 was included in large nuclear granules outside the nucleolar zone, clearly visible in the nuclei of the peripodium's cells (Figure 1M-M'). These large structures and the abnormal nucleolar morphology were rescued when NOC1-RNAi was co-expressed with HA-NOC1 (Figure 1L-L' and N-N').

NOC1 is important for rRNA processing, ribosome maturation and functional protein synthesis.

To investigate the role of *Drosophila*'s NOCs in ribosome biogenesis, we first analyzed the impact of NOC1 on ribosome maturation and protein synthesis. Polysome profiling in whole larvae showed that overexpression of NOC1 significantly increased the abundance of the 80S and polysomes peaks are increased compared to the WT (Figure 2A, B). On the contrary, NOC1 reduction resulted in a dramatic decrease in ribosomal subunits and polysomes abundance (Figure 2C) with a robust reduction of the 80S and the relative increase of the 40S and 60S subunits, suggesting a defect in ribosome recruitment on polysomes (Figure 2D, E). In yeast, the NOC1/NOC2 complex was shown to regulate the activity of Rpr5, an assembly factor that blocks the cleavage of the internal transcribed spacers (ITS) during the rRNA precursors maturation, a process necessary for the stoichiometric production of the two ribosomal subunits (Khoshnevis et al., 2019). To assess if *Drosophila* NOC1 also controlled this process, we quantified the levels of ITS1 and ITS2 and of the relative mature RNAs by qRT-PCR. This analysis showed that reduction of NOC1 induced the accumulation of the intermediate ITS1 and ITS2 immature forms of rRNAs with consequent reduction of the 18S and 28S rRNAs (Figure 2F). On the contrary, NOC1 overexpression only reduced the level of ITS1 but not of ITS2, and

significatively increased the amount of 18S and 28S rRNAs (Figure 2F). These data confirm that also in flies NOC1 is part of the mechanism that controls rRNAs synthesis and ribosomal processing. To evaluate whether these defects reflected changes in global protein synthesis, we performed a SUnSET (Surface Sensing of Translation) assay (Deliu et al., 2017). These experiments showed that in *NOC1-RNAi* animals the translation of labeled puromycin-peptides was robustly diminished compared to control animals (Figure 2G-I). On the contrary, overexpression of NOC1 did not significantly impair translation (not shown).

Reduction of NOC1, NOC2 and NOC3 during development limits growth in the eye by affecting the number and size of the ommatidia but does affect the size in differentiated ommatidia.

We then better characterized the role of NOCs *in vivo,* by analyzing the impact of their modulation of expression in organs that represent models for the growth of the animal. We started with an analysis of NOCs in tissues with different proliferative characteristics. We used the *GMR* promoter (Hay et al., 1994), to modulate NOCs expression at mid-third instar stage in the differentiated cells of the retina, and the *tubulin* promoter in combination with *eyeless*-flippase, to restrained the expression of NOCs to the proliferative cells precursors of the eye and antenna discs (Bellosta et al., 2005). These experiments showed that downregulation of NOC1, 2 or 3 or NOC1 overexpression (OE) in differentiated cells using the GMR promoter did not affect the eye morphology nor their size (Figure 3A-E, and Supplementary Figure 4A). On the contrary, downregulation of NOC1, 2 or 3 using the *tubulin* promoter, resulted in small eyes with smaller and disorganized ommatidia (Figure 3H-J and N and Supplementary Figure 4B) while no defect were observed with NOC1 overexpression (Figure 3G, and N). Moreover, the growth defect induced by NOC1-RNAi was rescued by co-expression of the inhibitor of caspase P35 (Figure 3L-M and O), indicating that the eye defects were the result of apoptosis.

Reduction of NOC1 in the prothoracic gland delays animal development by reducing ecdysone levels.

The prothoracic gland (PG) produces the hormone ecdysone that controls animal development (Nijhout et al., 2014). Reduction of NOCs using the *P0206-Gal4* promoter resulted to a delay in development (Valenza et al., 2018), these animals

never pupariated and continued to grow for about 20 days (Table 1) increasing the size of the cells in the fat bodies (Figure 4A-B)(Valenza et al., 2018). Macroscopic analysis of the PG in *NOC1-RNAi* animals did not reveal any morphological defects and at 5 days AEL its size was similar to that of control animals. However, at 12 days AEL the size of the PG in *NOC1-RNAi* animals was significantly atrophic (Figure 4D-F). We next determined the levels of ecdysone by indirectly measuring the expression of its target *Ecdysone-induced protein 74b mRNA (E74b)*. These data showed that *E74-mRNA* expression from whole larval tissues was already reduced at 5 days AEL in *NOC1-RNAi* animals compared to controls and it was further lowered at 12 days AEL (Figure 4C). On the contrary, NOC1 overexpression did not lead to any detectable changes in *E74b- mRNA* level or in change in larval body size (not shown).

NOC1 downregulation in the fat body reduces cell size and lipid storage resulting in dyslipidemia.

Lowering NOC1, 2, or 3 expression in flip-out clones analyzed in the fat body significantly reduced cell size and induced morphological defects (Figure 5C-E, and F). We then investigated the impact of reducing NOC1 in the whole organ using the *Cg (Collagene4a1)* (Parisi et al., 2013) and the *FB* promoters (Schmid et al., 2014). These experiments showed that reduction of NOCs in the fat body was lethal with similar results obtained using both promoters (Table 1). A more deeper analysis using the *Cg* promoter showed that reduction of NOC1 increased the timing of development (> than 24 hours) when compared to control animals, resulting in small larvae that eventually died between late third instar and at pupal stages (Figure 5G, Table 1); only a small percentage of animals (<10%) hatched as small adults when we used *NOC1-RNAi* expressed on chromosome II (Figure 5H), that was significantly less effective than the line on chromosome III in reducing *NOC1-mRNA* (Supplementary Figure 5A). On the contrary, overexpression of NOC1 increased larval volume, significative at 96 AEL, resulting in adults that hatched with a slightly bigger size than control, as shown by analysis of their wing size (Figure 5H). One function of the fat body is to store lipids and sugars necessary for the animal to develop and to survive metamorphosis. Analysis of the contents of triglycerides (TGAs) showed that *NOC1-RNAi* larvae had less lipids compared to wild type sibling animals taken at the same stage of development (Figure 5I). A morphological

analysis of the larval tissues using Nile Red to stain lipids, showed that the fat body near the salivary glands (sg) was almost absent in *NOC1-RNAi* animals (Figure 5J and N). Indeed, we observed that *NOC1-RNAi* animals accumulated high level of lipids in the gut (Figure 5K and O), in the brain and in the imaginal discs (Figure 5L and P). This is a response for the reduced lipid-storage capability of these animals that induce dyslipidemia, an inter-organ process active when fat cells fail to properly store lipids and non-autonomously stimulate other organs to accumulate them (Palm et al., 2012).

The fat body also remotely controls the release of *Drosophila* insulin-like peptides (DILP2, 3 and 5) from the Insulin Producing Cells (IPCs), that are normally secreted in the hemolymph in response to nutrients or retained when the animal undergos to starvation (Geminard et al., 2009). Analysis of DILP2 expression in the IPCs showed that, even in adequate nutrients conditions (FED), DILP2 was retained in the IPCs of animals with reduced NOC1 in the fat body (Figure 5M-Q), suggesting that these animals lost the ability to remotely control the release of DILPs, thus mimicking starvation, a condition in which DILPs would ordinarily be retained.

NOC1 reduction in cells of the wing imaginal disc results in cell death and induces cell competition that is partially rescued in a Minute/+ background.

To assess the impact of NOCs on the growth of epithelial cells, we generated flip-out clones where NOCs level was either reduced or overexpressed and GFP was co-expressed as a cellular marker. Clones were induced at 48 hrs AEL and analysis of their size and number was performed between 72-90 hrs AEL in wing imaginal discs. This analysis showed that NOC1 overexpression did not significantly alter cell morphology or size, and clones developed at similar rate to control cells expressing only GFP (Figure 6A-B, J). Instead, NOCs downregulation caused a significant reduction in the number and size of the clones, and the few that we found contained smaller cells with morphology reminiscent of dying cells (Figure 6C-E, J). Further analysis showed that *NOC1-RNAi* clones induced at 48 hours AEL were not detected when analyzed at 90 hrs. AEL (Figure 6G, H), while control GFP clones reached the size of about 120 cells/clone (Figure 6F-H). Only when clones were induced at 72 AEL we were able to score few *NOC1-RNAi* clones that were still significantly smaller than control and partially rescued when the inhibitor of caspase P35 was co-expressed (Figure 6K-M). The size of the *NOC1-RNAi* clones was

overall 15% the size of wild type GFP clones, considered 100% (Figure 6K-L, I), and co-expression of P35 was able to partially rescue *NOC1-RNAi* clonal-size up to 60% (Figure 6M, I). These results suggest that cells with reduced NOC1 might be eliminated by the neighboring cells by cell competition, a mechanism described for ribosomal proteins of the *Minute* family. in which cells with reduced protein synthesis were killed and outcompeted by the wild-type neighboring cells. To understand if *NOC1-RNAi* was triggering cell competition we induced *NOC1-RNAi* clones in animals heterozygotes for the *Minute (3)66D* gene that carries a mutation in the gene encoding for the ribosomal protein RpL14 (Saeboe-Larssen et al., 1997). These experiments showed that *NOC1-RNAi* clones were partially rescued in their number and size when induced in a *Minute* heterozygous background (Figure 6N-O), suggesting that NOC1 is part of the mechanisms regulating ribosomal proteins-induced cell competition.

Reduction of NOC1 induces eiger/JNK pathways resulting in apoptosis and DILP8 upregulation that depends on XRP1 activation.

We further characterize the mechanisms underlining NOC1-RNAi-induced apoptosis in epithelial cells of the wing imaginal discs. We started this analysis using the *MS1096* dorsal wing promoter (Capdevila and Guerrero, 1994) and showed that both overexpression of NOC1 and its reduction did not significantly affected the morphology of the discs, that exhibited the correct pattern for Wingless expression (Figure 7A-C). However, when we analyzed the timing of larval development, we observed that *NOC1-RNAi* animals developed to a smaller size than control with a significant difference at 120hrs AEL (Figure 7D). These larvae were delayed in their development and reached pupariation 24 hr. late in respect to larvae from control or *NOC1-OE* animals (Figure 7E, and Table 1). In addition, reduction of NOC1 using the RNAi line on Chromosome III resulted in pupal lethality, while using the line on Chromosome II resulted in <10% of animals that hatched with wings that presented morphological defects in the dorsal side and were significantly smaller (Figure 7F-H and Supplementary Figure 5B). The combination of developmental delay and apoptosis prompted us to check if the reduction of NOC1 upregulates DILP8, that is normally secreted in response to cell death and tissue damage. Indeed, we found *Dilp8*-mRNA significantly increased (>40 x) in these larvae (p<0.01), whereas its level was not changed upon NOC1 overexpression (not shown).

To better analyze at cellular level the mechanism underlying Dilp8 upregulation, we reduced NOC1 using the wing specific *rotund-Gal4* promoter. These experiments confirmed that in cells where NOC1 was reduced the level of *dilp8*-GFP increased (Figure 7I-J) (similar results were obtained using the *MS1096* promoter – not shown). Concomitantly, we found an upregulation of the pro-apoptotic gene *eiger* using its reporter *eiger-GFP* (Figure 7N-O), that was accompanied with an activation of JNK signaling indicated by the increase in *TRE-dsRED* (Figure 7R-S). In agreement with these results, anti-Caspase3 staining indicated that apoptosis was significantly increased in cells with reduced NOC1 (Figure 7V-W). Cells undergoing proteotoxic stress are subjected to elimination by cell competition with a mechanism that depends on Xrp1, a transcription factor upregulated in Rp-/+ conditions. Notably, we found that *NOC1-RNAi* cells transcriptionally upregulated Xrp1 analyzed using *Xrp1*^{02515}*-LacZ* reporter line (Baillon et al., 2018)(Supplementary Figure 6). These data strongly suggest that cells with reduced NOC1 undergo proteotoxic stress with upregulation of *Xrp1* and *eiger,* causing cell damage that activates the DILP8/Lgr3 compensatory mechanism, responsible for the developmental delay observed in *NOC1-RNAi* animals. We then performed epistasis experiments to better determine the roles of Xrp1 and eiger in activating Dilp8 response. Unfortunately, the contemporary reduction of NOC1 and Xrp1 using either *rotund* or *nubbin* promoters resulted in embryonic lethality, while larvae with both NOC1 and eiger downregulation using the same promoters were viable. We therefore verified the possible dependance of Dilp8 upregulation on eiger both by quantification of GFP by imaging of *dilp8*-GFP using for chromosomal convenience the *nubbin*-promoter (Figure 7K-L and P-Q) and by qRT-PCR. These experiments showed that upon reduction of NOC1 and eiger, a partial but not significant decrease of Dilp8-GFP levels was observed in the wing imaginal discs (Figure 7K-L, and P-Q and M), data that were confirmed also by qRT-PCR of *Dilp8-mRNA* that was not significantly changed when eiger level was reduced by RNA interference (Figure 7T and Supplementary Figure 7). Moreover, *Xrp1-mRNA* levels, which are increased upon NOC1 downregulation, are not reduced in imaginal discs from *NOC1-RNAi; eiger-RNAi* animals (Figure 7U). Overall, these results suggest that Dilp8 expression is predominantly controlled by Xrp1 and point to a more upstream role for Xrp1 in respect to eiger in controlling the proteotoxic response following reduction of NOC1.

Discussion

We have shown that the yeast homologs NOC1, NOC2 and NOC3 of Drosophila (Figure 1A) are required for animal development and their ubiquitous reduction results in growth impairment and larval lethality (Figure 1B and Table 1). NOC1 ubiquitous overexpression is also detrimental but at pupal stage, a phenotype that is rescued by co-expression of NOC1-RNAi that allows the animals to develop to small adults (Figure 1C-E). These data suggest that NOC1 expression must be tightly regulated, as either its reduction or overexpression may be detrimental for the cells. As demonstrated in yeast, *Drosophila* NOC1 function is not redundant, and its overexpression does not compensate for the loss of *NOC2* and *NOC3* (not shown). The reason for this behavior may be that NOC proteins function as heterodimers (NOC1/NOC2 and NOC2/NOC3) that are necessary for proper control of rRNA processing and the assembling of the 60S ribosomal subunits (Edskes et al., 1998; Hierlmeier et al., 2013; Milkereit et al., 2001). Indeed, it was demonstrated in yeast that NOC1/NOC2 complex regulates the activity of the Ribosomal RNA protein-5 (Rpr5) that controls rRNA cleavage at the internal transcribed spacers ITS1 and ITS2 sequences to ensure the stoichiometric maturation of the 40S and 60S ribosomal subunits (Khoshnevis et al., 2019). This function is likely to be conserved also in flies. In fact, our results show that reduction of NOC1 induces the accumulation of the intermediate ITS1 and ITS2 immature forms of rRNAs. Moreover, we observed a reduction in the relative abundance of 18S and 28S rRNAs (Figure 2F), suggesting that NOC1 is required also in flies for proper rRNA processing and ribosome maturation (Milkereit et al., 2001). In line with this hypothesis, we demonstrated that NOC1 reduction results in a strong decrease in ribosome abundance and assembling, also accompanied by a strong reduction of the 80S and the polysomes (Figure 2C). In addition, we also observed a mild accumulation of the 40S and 60S subunits (Figure 2D and E), suggesting that the mature 80S ribosome might be unstable in NOC1-RNAi animals and that a small percentage of the ribosome disassembles in the two subunits, leading to the observed increase. In addition, since NOC1 was identified as a predicted transcription factor (Kudron et al., 2018; Neumuller et al., 2013; Port et al., 2020), and because reduction of NOC1 results to a robust decrease in global protein synthesis (Figure 2G-H), we cannot exclude that specific factors involved in the 80S assembling are reduced or missing in NOC1-RNAi animals.

Analysis of protein-protein interaction using STRING indicates that CG7838/NOC1 may act in a complex with other nucleolar proteins (Supplementary Figure 1). Indeed, here we showed that NOC1 colocalizes in the nucleolus with fibrillarin (Figure 1I, K and M). Moreover, NOC1 overexpression also results in the formation of large rounded nuclear structures, that are significantly reduced when its expression is decreased by NOC1-RNAi (Figure 1K'-L' and M'-N'). Interestingly, similar structures have been shown for CEBPz, the human homologue of NOC1 visible in images from "The Human Protein Atlas". CEBPz (also called CBF2, CTF2) (OMIM-612828) is a transcription factor member of the CAAT-Binding proteins, involved in the complex of H*sp70* activation (Lum et al., 1990) and found upregulated in tumors, particularly in cells from patients with Acute Myeloid Leukemia (AML) (Herold et al., 2014). The presence also in NOC1 of the conserved CBP domain (Figure 1A) suggests that it may also act as putative transcription factor, hypothesis corroborated by metadata in *Drosophila* (CHIP-Seq and genetic screens) that demonstrate how its expression is associated to promoter regions of genes with a function in the regulation of nucleolar activity and of ribosomal proteins (Neumuller et al., 2013; Shokri et al., 2019). This observation is important as it opens the possibility that NOC1 can control ribosome biogenesis through alternative mechanisms in addition to its control over rRNA transport and maturation. Moreover, we believe this function may be conserved for CEBPz, since in our bioinformatic analysis we identified nucleolar components and ribosomal proteins being upregulated in liver and breast tumors with an overexpression of CEBPz (Supplementary Table 1). Interestingly, misexpression of some of these targets, like Rpl5 and Rpl35a, have been associated to ribosomopathies suggesting the possibility that mutations in CEBPz could contribute to tumorigenesis in these genetic diseases (Mills and Green, 2017; Narla and Ebert, 2010).

To better characterize NOC1 functions *in vivo* we modulated its expression in organs that are relevant for *Drosophila* physiology, such as the prothoracic gland (PG), the fat body (FB) and the wing imaginal discs.

Prothoracic gland (PG)

While the overexpression of NOC1 in the prothoracic gland (PG) does not affect development, its reduction significantly decreases ecdysone production, as shown by *E74b* mRNA levels (Figure 4C). This reduction is significant both at 5 and at 12 days AEL when occurs concomitantly with the reduction of the PG size (Figure 4F). Consequently, *NOC1-RNAi* animals are developmentally delayed and do not undergo pupariation but rather continue to wander until they die at about 20 days AEL (Figure 4A). These animals feed constantly and increase their size, accumulating fats and sugars in the fat body's cells that augment their size (Figure 4B). We previously described the presence of hemocytes (macrophage-like cells) infiltrating the fat body of these animals, a condition accompanied with an increase in JNK signaling and ROS (Reactive Oxygen Species), likely released by the fat cells under stress condition (Valenza et al., 2018). Interestingly, this inter-cellular event recapitulates the chronic low-grade inflammation, or Adipocyte Tissue Macrophage (ATM), a pathology associated to adipose tissue in obese people (Horng and Hotamisligil, 2011) that represents the consequence of impaired lipid metabolism.

Fat body

Reduction of NOC1, 2 or 3 in the fat body results in smaller and fewer cells (Figure 5C-E and F), while reduction of NOC1 in the whole organ inhibits animal development (Table 1). The fat body regulates animal growth by sensing amino acids concentrations in the hemolymph and remotely controlling the release of DILP2, 3 and 5 from the Insulin Producing Cells (IPCs) (Andersen et al., 2013; Geminard et al., 2009; Hyun, 2018). The fat body also functions as storage of nutrients (fats and sugars) necessary during the catabolic process of autophagy that allows animals to survive metamorphosis (Rusten et al., 2004; Scott et al., 2004). When nutrients are limited, larvae delay their developmental to accumulate fats and sugars until reaching their critical size, that ensures them to progress through metamorphosis (Hironaka et al., 2019; Texada et al., 2020). NOC1 downregulation in the fat alters their ability to store nutrients, and larvae proceed poorly through development (Figure 5G). In addition, these animals show DILP2 accumulation in the IPCs even in normal feeding conditions (Figure 5Q), indicating that the remote signals responsible for DILPs release are greatly reduced, phenocopying animals in

starvation or with reduced levels of MYC in fat cells (Geminard et al., 2009; Parisi et al., 2013). Interestingly, we also observed that *Cg-NOC1-RNAi* animals accumulate an abnormal amount of fats in non-metabolic organs such as gut, brain, and imaginal discs (Figure 5O-P). This finding suggests that these animals are subjected to inter-organ dyslipidemia, a mechanism of lipids transport activated when the fat body is impaired, which triggers non-autonomous signals to induce other organs to store fats. Interestingly, this condition recapitulates dyslipidemia in humans, where the compromised adipose tissue releases lipoproteins of the APO family inducing fat accumulation in organs (Pirillo et al., 2021). Notably, a similar condition was described also in flies for mutations in members of the *APOE* family (Palm et al., 2012), outlining how the mechanisms controlling the inter-organ fat metabolism are conserved among species.

Wing imaginal discs

NOC1 depletion in clones analyzed in the wing imaginal discs triggers their elimination by apoptosis (Figure 6K-M). This event is partially rescued when clones are induced in the hypomorphic background of the *Minute(3)66D/+* mutation (Saeboe-Larssen et al., 1997) (Figure 6N-O). These cells also upregulate the pro-apoptotic gene Xrp1 (Figure 7U and Supplementary Figure 6), recently shown to be responsible for controlling translation and indirectly cell competition upon proteotoxic stress (Baillon et al., 2018; Baumgartner et al., 2021; Kiparaki et al., 2022). Reduction of NOC1 in the wing imaginal disc prolongs larval development (Figure 7D-E) with upregulation of DILP8 (Figure 7I-J, K-L and M) normally induced by cellular damage and apoptosis. The fact that NOC1-RNAi cells upregulate, in addition to Xrp1, *eiger* (Figure 7N-O), another pro-apoptotic gene and member of the TNFα family and activate JNK pathway (Figure 7R-S), suggests that different mechanisms are converging in these cells to induce apoptosis and DILP8 upregulation. We performed genetic epistasis to define in deep the relation between eiger signaling in NOC1-RNAi cells and how this is linked to Xrp1 transcriptional upregulation in response to nucleolar stress and DILP8 upregulation. This analysis showed that reduction of eiger did not significantly affect Dilp8 expression induced upon NOC1 downregulation (Figure 7L-Q, M). Due to the embryonic lethality induced by the simultaneous reduction of NOC1 and Xrp1 in cells of the wing

imaginal discs, using both *rotund* or *nubbin* promoters, we analyzed the contribute of eiger to Xrp1 and Dilp8 transcriptional regulation upon NOC1-RNAi. These data indicate that Dilp8 upregulation was not significantly affected by the reduction of eiger upon NOC1 reduction (Figure 7T), confirming the data in vivo with dilp8-GFP. In addition, we can predict that Xrp1 acts independently of eiger, since *Xrp1-mRNA* upregulation is not rescued in imaginal discs from *NOC1-RNAi; eiger-RNAi* animals (Figure 7U), pointing out to a more upstream role for Xrp1 in controlling the stress response following reduction of NOC1 while eiger function remains to be determined.

In conclusion, our data corroborate the role of NOC1 in the mechanisms that induce proteotoxic stress adding NOC1 as a novel component that links defects in protein synthesis with cell competition. We also showed the relevance of NOC1 in promoting nucleolar stress and apoptosis, both leading cause of tumor formation (Penzo et al., 2019; Quin et al., 2014). Our data support a potential role for the human homologue CEBPz in the context of tumorigenesis. Indeed, mutations in CEBPz are described in >1.5% of tumors of epithelial origins (cBioPortal), suggesting that it may have a role in contributing to the signals that trigger proteotoxic stress associated to tumorigenesis (Mills and Green, 2017; Narla and Ebert, 2010). CEBPz was also found together with the METTL3-METTL14 methyltransferase complex to control cellular growth (Barbieri et al., 2017) and in the regulation of H3K9m3 histone methylation in response to srHC (sonication-resistant heterochromatin), highlighting a role as moonlight protein for this transcription factor also in RNA and heterochromatin modifications (McCarthy et al., 2021).

Materials and Methods

Drosophila husbandry and lines

Animals were raised at low density in vials containing standard fly food, composed of 9g/L agar, 75 g/L corn flour, 50 g/L fresh yeast, 30g/L yeast extract, 50 g/L white sugar and 30 mL/L molasses, along with nipagine (in ethanol) and propionic acid. The crosses and flies used for the experiments are kept at 25°C, unless otherwise stated.

The following fly lines were used: *GMR-Gal4* (Parisi et al., 2011), *tub>y+>Gal4; ey-flp* (Bellosta et al., 2005), *P0206-GFP-Gal4* (Valenza et al., 2018), the fat body specific promoter *FB-Gal4* (kind gift from Ines Anderl, University of Tampere, Finland,) *rotund-Gal4* and *yw; nubbin>Gal4* (kind gift from Hugo Stocker, ETH Zurich, CH), *actin-Gal4,GFP/Gla*,*Bla* (kind gift from Daniela Grifoni University of l' Aquila, IT), *yw; Actin>CD2>Gal4,GFP/TM6b* (kind gift from Bruce Edgar, University of Boulder, CO), *MS1096-Gal4* (kind gift from Erika Bach, NYU, USA), *Minute(3)66D/+ (Saeboe-Larssen et al., 1997), engrailed-Gal4* (kind gift from Gary Struhl, Columbia University), *Xrp1-LacZ* (kind gift from Koni Basler, University of Zurich) and *actin-Gal4, GFP; tub-Gal80ts* originated in this work. The following stocks were obtained from the Bloomington *Drosophila* Stock Center: *Cg-Gal4.A2* (B7011), *elav-Gal4* (B458), *UAS-CG7839-RNAi (B25992*), *UAS-CG9246-RNAi* (B50907), *UAS-CG1234-RNAi* (B61872), *CG7839-GFP.FTPD* (B51967), *dilp8-GFPMI00727* (B33079), *TRE-dsRedT4* (B59011); and from the Vienna *Drosophila* Resource Center: *UAS-CG7839-RNAi* (v12691), *sgRNA^{CG7839}-CFDlib01132* (v341898), *hh-Gal4;uMCas9* (v340019), *w^{1118}* (v60000), *UAS-eiger-RNAi* (v45253), *eiger-GFP-2XTY1-SGFP-V5-preTEV-BLRP-3XFLAG* (v318615); and from FlyORF (ZH) the line *UAS-CG7839-3xHA* (F001775).

Measurement of larval length and volume

Larvae at the indicated stage of development and genotypes were anesthetized using freezing cold temperature, and pictures were taken using a Leica MZ16F stereomicroscope. Width and length were measured using a grid and volume was calculated by applying the formula in (Parisi et al., 2013).

Quantitative RT-PCR

RNA extraction was performed using the RNeasy Mini Kit (Qiagen), following the manufacturer instructions. The isolated RNA was quantified with the Nanodrop2000. 1000 ng of total RNA were retrotranscribed into complementary DNA (cDNA) using the SuperScript IV VILO Master Mix (Invitrogen). The obtained cDNA was used for qRT-PCR using the SYBR Green PCR Kit (Qiagen). The assays were performed on a BioRad CFX96 machine and the analysis were done using Bio-Rad CFX Manager software. Transcript abundance was normalized using *actin5c*. The list of the primers is available in Table 2.

Dissection and immunofluorescence

Larvae were collected at the third instar stage, dissected in 1x phosphate-buffered saline (PBS), and fixed for 30 minutes in 4% paraformaldehyde (PFA) at room temperature (RT). After 15 minutes of tissue permeabilization with 0.3% Triton X-100, samples were washed in PBS-0.04% Tween20 (PBST) and blocked in 1% bovine serum albumin (BSA) for 1 hour at RT. Samples were incubated overnight at 4°C with primary antibodies in 1% BSA and, after washing, with Alexa-Fluor 488 or 555-conjugated secondary antibodies 1:2000 in BSA. During washing in PBST nuclei were stained with Hoechst. Imaginal discs were dissected from the carcasses and mounted on slides with Vectashield (LsBio-Vector Laboratories). Imagines were acquired using a Leica SP5 and SP8 confocal microscopes and assembled using Photoshop2020 from Adobe Creative Clouds. Primary antibodies used: rat anti-HA 1:1000 (Roche 3f10), mouse anti-fibrillarin (1:100) (ABCAM ab4566), mouse anti WG 1:100 (DSHB 4D4), rabbit anti-cleaved Caspase3 1:400 (Cell Signaling 9661). Fluorescence intensity was determined by measuring the mean grey value in the wing pouch with ImageJ software.

Western blot

Proteins were extracted from third instar larvae collected in 250 ul of lysis buffer (50 mM Hepes pH 7.4, 250 mM NaCl, 1 mM EDTA, 1.5% Triton X-100) containing a cocktail of phosphatases and proteases inhibitors (Roche). Samples were run on a SDS-polyacrylamide gel and then transferred to a nitrocellulose membrane. After blocking with 5% non-fat milk in TBS-Tween, membranes were incubated with primary antibodies against puromycin 1:1000 (clone 12D10 MABE343, Merk), mouse anti-HA 1:200 (supernatant Sigma HA7) and anti-actin 1:200 (DSHB 224-236-1), followed by incubation with HRP conjugated secondary antibodies (Santa Cruz Biotechnology), and signal was detected using ECL LiteAblot Plus (Euroclone) and the UVITec Alliance LD2.

SUnSET assay

UAS-NOC1-RNAi was expressed ubiquitously in whole larvae using the *actin-Gal4* coupled with *tubulin-Gal80* temp sensitive allele to avoid early lethality. Crosses were kept at 18°C and when larvae reached second instar were switched to 30°C for 72 hours prior to dissection. At least seven third-instar larvae for each genotype were

dissected in Schneider's medium and then transferred to Eppendorf tubes containing complete medium with 10 % serum plus puromycin at 20 µg/ml (Invitrogen, Thermo Fisher Scientific). The samples were incubated for 40 or 60 minutes at room temperature, then recovered in 10% serum/media without puromycin for 30 minutes at room temperature. After the inverted larvae were snap frozen in liquid nitrogen for subsequent western blot analysis using anti-puromycin primary antibody.

Polysome profiling

Cytoplasmic lysates were obtained from snap-frozen whole larvae pulverized using liquid nitrogen. After addition of lysis buffer and centrifugations for removal of the debris, cleared supernatants were loaded on a linear 10%–40% sucrose gradient and ultracentrifuged in a SW41Ti rotor (Beckman) for 1 hour and 30 min at 270,000 *g* at 4°C in a Beckman Optima LE-80K Ultracentrifuge. After ultracentrifugation, gradients were fractionated in 1 mL volume fractions with continuous monitoring of absorbance at 254 nm using an ISCO UA-6 UV detector. % of ribosomal subunits was calculated over the (40, 60, 80 and polysome) area of the same genotype.

Generation of inducible flip-out clones and clonal analysis.

Females, *yw; Actin>CD2>Gal4-GFP/TM6b* were crossed with males carrying the heat-shock *Flippase* y^{122}*w* together with the relative UAS-transgenes. Animals were left laying eggs for 3-4 hours. Heat shock was performed on larvae at 48 or 72 hours after egg laying (AEL) for 15 min at 37°C. Larvae were dissected at 96 or at 120 hours AEL and mounted using MOWIOL. Images of clones expressing nuclear GFP were acquired using a LEICA SP8 confocal microscope. Quantification of the number of GFP-positive cells/clone in the wing imaginal discs was calculated from 5 confocal images for every genotype at 40x magnification maintaining constant acquisition parameters. Co-staining with phalloidin-Rhodamine (Invitrogen) was necessary in Figure 5 A-E to outline the cell membranes and DAPI for the nuclei.

Imaging the adult compound eye and wings

Photographs of eyes of adult female expressing the indicated UAS-transgenes in the retina using the *GMR-Gal4 or tub>y+>Gal4* promoters were taken at 8 days after eclosion using a Leica stereomicroscope MZ16F at 4x magnification. 2-4-days old

animals were fixed in a solution of 1:1 glycerol and ethanol. One wing was dissected from at least 10 animals and mounted on a slide in the same fixing solution. Images of each wing were taken using a Zeiss Axio Imager M2 microscope with a 1x magnification. Quantification of the area of each wing and eye was performed on photographs using PhotoshopCS4.

Fat body staining and cell size calculation

Fat bodies were dissected from larvae at 5 or 12 days AEL fixed in 4% PFA and counterstained with Nile Red (Sigma), Phalloidin-488 (Invitrogen) and Hoechst 33258 (Sigma). After washing with PBS, fat bodies were mounted onto slides with DABCO-Mowiol (Sigma-Aldrich) and images were acquired using LeicaSP5-LEICA, the area of adipose cells for each fat body was calculated with ImageJ software. Measurement of TAGs and visualization of lipids in the whole larvae was done as in (Parisi et al., 2013) using Nile Red staining. Dissected organs were mounted in DABCO-Mowiol and photographs were taken using a Zeiss Axio M2 Imager light microscope.

Generation of CRISPR-Cas9 mutations of *Noc1/CG7839* and analysis of their function in the posterior compartment of wing imaginal disc.

To target mutations in CG7839 into the germ line we crossed the line nos-Gal4VP16 UAS-uMCas9(attP40) with the line *gRNA* for *CG7839* (*vCFDlib01132*) from Boutros collection (Port et al., 2020). Out of 30 putative lines carrying potential NOC1 heterozygous mutations, we sequenced five lines and two of them contained indels that create nonsense mutations that translated *NOC1-mRNAs* into short NOC1 polypeptidic sequences of 30 amino acids (NOC1-mut^{12}) and 29 amino acids (NOC1-mut^{14}). Sequences of the primers used for the screening are in Table 2. Phenotypic analysis of NOC1-mutant homozygous larvae was carried by leaving heterozygous *w^{1118}; NOC1-mutant/TM6b* parents to lay eggs for 5 hrs. at 25°C in regular food. Homozygous not *tubby* larvae were scored, and pictures were taken at 8 days AEL. At this stage heterozygous *NOC1/TM6b* larvae were all pupae that hatched at the expected time. Mutations of *CG7938* were targeted in the posterior compartment of the wing imaginal disc by using the line *UAS-uMCas9; hh-Gal4/TM6B* to spatially limit the transcription of Cas9 in the posterior region of the animal under *hh-Gal4* (Port et al., 2020). This line was crossed with that carrying the

sgRNA for *CG7839* (*vCFDlib01132*) previously recombined with *UAS-GFP* to mark the posterior compartment. A line expressing only *UAS-GFP* was used as control. F1 animals were dissected at about 90 hours AEL and images of their wing imaginal discs were acquired using a confocal microscope (Leica SP8). Calculation of the size of the posterior compartment (GFP-positive) and the total area of the wing imaginal discs were performed using Adobe Photoshop (Creative Cloud). At least 8 animals from each genotype were used for the statistical analysis.

Statistical Analysis

Student *t*-test analysis and analysis of the variance calculated using one-way ANOVA with Tukey multi-comparisons test were calculated using GraphPad-PRISM*8. p* values are indicated with asterisks *** =** $p < 0.05$, ** = $p < 0.01$, *** = $p < 0.001$, **** = $p < 0.0001$, respectively.

Acknowledgements

We thank Marcello Ceci for reading the manuscript and for the useful discussion, the Advanced Imaging Core Facility at CIBIO, the Vienna VDRC and Bloomington Stocks Centers and the DSHB for antibodies. Stocks obtained from the Bloomington Drosophila Stock Center (NIH P40OD018537) were used in this study.

We apology in advance to any authors whose work has been omitted. Department CIBIO Core Facilities are supported by the European Regional Development Fund (ERDF) 2014–2020.

Competing interest

No competing interest declared

Funding

This work was supported by the NIH Public Health Service grant from the NIH-SC1DK085047 to PB and SZ, MAE PGR00155 to EMP.

Data availability none

References

Akai, N., Ohsawa, S., Sando, Y. and Igaki, T. (2021). Epithelial cell-turnover ensures robust coordination of tissue growth in Drosophila ribosomal protein mutants. *PLoS Genet* **17**, e1009300.

Andersen, D. S., Colombani, J. and Leopold, P. (2013). Coordination of organ growth: principles and outstanding questions from the world of insects. *Trends Cell Biol* **23**, 336-44.

Baillon, L., Germani, F., Rockel, C., Hilchenbach, J. and Basler, K. (2018). Xrp1 is a transcription factor required for cell competition-driven elimination of loser cells. *Sci Rep* **8**, 17712.

Baral, S. S., Lieux, M. E. and DiMario, P. J. (2020). Nucleolar stress in Drosophila neuroblasts, a model for human ribosomopathies. *Biol Open* **9**.

Barbieri, I., Tzelepis, K., Pandolfini, L., Shi, J., Millan-Zambrano, G., Robson, S. C., Aspris, D., Migliori, V., Bannister, A. J., Han, N. et al. (2017). Promoter-bound METTL3 maintains myeloid leukaemia by m(6)A-dependent translation control. *Nature* **552**, 126-131.

Barna, M., Pusic, A., Zollo, O., Costa, M., Kondrashov, N., Rego, E., Rao, P. H. and Ruggero, D. (2008). Suppression of Myc oncogenic activity by ribosomal protein haploinsufficiency. *Nature* **456**, 971-5.

Baumgartner, M. E., Dinan, M. P., Langton, P. F., Kucinski, I. and Piddini, E. (2021). Proteotoxic stress is a driver of the loser status and cell competition. *Nat Cell Biol* **23**, 136-146.

Bellosta, P., Hulf, T., Balla Diop, S., Usseglio, F., Pradel, J., Aragnol, D. and Gallant, P. (2005). Myc interacts genetically with Tip48/Reptin and Tip49/Pontin to control growth and proliferation during Drosophila development. *Proc Natl Acad Sci U S A* **102**, 11799-804.

Boulan, L. and Leopold, P. (2021). What determines organ size during development and regeneration? *Development* **148**.

Brown, B., Mitra, S., Roach, F. D., Vasudevan, D. and Ryoo, H. D. (2021). The transcription factor Xrp1 is required for PERK-mediated antioxidant gene induction in Drosophila. *Elife* **10**.

Capdevila, J. and Guerrero, I. (1994). Targeted expression of the signaling molecule decapentaplegic induces pattern duplications and growth alterations in Drosophila wings. *EMBO J* **13**, 4459-68.

Deliu, L. P., Ghosh, A. and Grewal, S. S. (2017). Investigation of protein synthesis in Drosophila larvae using puromycin labelling. *Biol Open* **6**, 1229-1234.

Destefanis, F., Manara, V. and Bellosta, P. (2020). Myc as a Regulator of Ribosome Biogenesis and Cell Competition: A Link to Cancer. *Int J Mol Sci* **21**.

Edskes, H. K., Ohtake, Y. and Wickner, R. B. (1998). Mak21p of Saccharomyces cerevisiae, a homolog of human CAATT-binding protein, is essential for 60 S ribosomal subunit biogenesis. *J Biol Chem* **273**, 28912-20.

Garelli, A., Heredia, F., Casimiro, A. P., Macedo, A., Nunes, C., Garcez, M., Dias, A. R., Volonte, Y. A., Uhlmann, T., Caparros, E. et al. (2015). Dilp8 requires the neuronal relaxin receptor Lgr3 to couple growth to developmental timing. *Nat Commun* **6**, 8732.

Geminard, C., Rulifson, E. J. and Leopold, P. (2009). Remote control of insulin secretion by fat cells in Drosophila. *Cell Metab* **10**, 199-207.

Grewal, S. S., Li, L., Orian, A., Eisenman, R. N. and Edgar, B. A. (2005). Myc-dependent regulation of ribosomal RNA synthesis during Drosophila development. *Nat Cell Biol* **7**, 295-302.

Hay, B. A., Wolff, T. and Rubin, G. M. (1994). Expression of baculovirus P35 prevents cell death in Drosophila. *Development* **120**, 2121-9.

Herold, T., Metzeler, K. H., Vosberg, S., Hartmann, L., Rollig, C., Stolzel, F., Schneider, S., Hubmann, M., Zellmeier, E., Ksienzyk, B. et al. (2014). Isolated trisomy 13 defines a homogeneous AML subgroup with high frequency of mutations in spliceosome genes and poor prognosis. *Blood* **124**, 1304-11.

Hierlmeier, T., Merl, J., Sauert, M., Perez-Fernandez, J., Schultz, P., Bruckmann, A., Hamperl, S., Ohmayer, U., Rachel, R., Jacob, A. et al. (2013). Rrp5p, Noc1p and Noc2p form a protein module which is part of early large ribosomal subunit precursors in S. cerevisiae. *Nucleic Acids Res* **41**, 1191-210.

Hironaka, K. I., Fujimoto, K. and Nishimura, T. (2019). Optimal Scaling of Critical Size for Metamorphosis in the Genus Drosophila. *iScience* **20**, 348-358.

Horng, T. and Hotamisligil, G. S. (2011). Linking the inflammasome to obesity-related disease. *Nat Med* **17**, 164-5.

Hyun, S. (2018). Body size regulation by maturation steroid hormones: a Drosophila perspective. *Front Zool* **15**, 44.

Ji, Z., Kiparaki, M., Folgado, V., Kumar, A., Blanco, J., Rimesso, G., Chuen, J., Liu, Y., Zheng, D. and Baker, N. E. (2019). Drosophila RpS12 controls translation, growth, and cell competition through Xrp1. *PLoS Genet* **15**, e1008513.

Johnston, L. A., Prober, D. A., Edgar, B. A., Eisenman, R. N. and Gallant, P. (1999). Drosophila myc regulates cellular growth during development. *Cell* **98**, 779-90.

Khoshnevis, S., Liu, X., Dattolo, M. D. and Karbstein, K. (2019). Rrp5 establishes a checkpoint for 60S assembly during 40S maturation. *RNA* **25**, 1164-1176.

Kiparaki, M., Khan, C., Folgado-Marco, V., Chuen, J., Moulos, P. and Baker, N. E. (2022). The transcription factor Xrp1 orchestrates both reduced translation and cell competition upon defective ribosome assembly or function. *Elife* **11**.

Koyama, T., Texada, M. J., Halberg, K. A. and Rewitz, K. (2020). Metabolism and growth adaptation to environmental conditions in Drosophila. *Cell Mol Life Sci* **77**, 4523-4551.

Kucinski, I., Dinan, M., Kolahgar, G. and Piddini, E. (2017). Chronic activation of JNK JAK/STAT and oxidative stress signalling causes the loser cell status. *Nat Commun* **8**, 136.

Kudron, M. M., Victorsen, A., Gevirtzman, L., Hillier, L. W., Fisher, W. W., Vafeados, D., Kirkey, M., Hammonds, A. S., Gersch, J., Ammouri, H. et al. (2018). The ModERN Resource: Genome-Wide Binding Profiles for Hundreds of Drosophila and Caenorhabditis elegans Transcription Factors. *Genetics* **208**, 937-949.

Langton, P. F., Baumgartner, M. E., Logeay, R. and Piddini, E. (2021). Xrp1 and Irbp18 trigger a feed-forward loop of proteotoxic stress to induce the loser status. *PLoS Genet* **17**, e1009946.

Lee, C. H., Kiparaki, M., Blanco, J., Folgado, V., Ji, Z., Kumar, A., Rimesso, G. and Baker, N. E. (2018). A Regulatory Response to Ribosomal Protein Mutations Controls Translation, Growth, and Cell Competition. *Dev Cell* **46**, 456-469 e4.

Li, N., Yuan, L., Liu, N., Shi, D., Li, X., Tang, Z., Liu, J., Sundaresan, V. and Yang, W. C. (2009). SLOW WALKER2, a NOC1/MAK21 homologue, is essential for coordinated cell cycle progression during female gametophyte development in Arabidopsis. *Plant Physiol* **151**, 1486-97.

Liu, Y., Mattila, J., Ventelä, S., Yadav, L., Zhang, W., Lamichane, N., Sundström, J., Kauko, O., Grénman, R., Varjosalo, M. et al. (2017). PWP1 Mediates Nutrient-Dependent Growth Control through Nucleolar Regulation of Ribosomal Gene Expression. *Dev Cell* **43**, 240-252.e5.

Lum, L. S., Sultzman, L. A., Kaufman, R. J., Linzer, D. I. and Wu, B. J. (1990). A cloned human CCAAT-box-binding factor stimulates transcription from the human hsp70 promoter. *Mol Cell Biol* **10**, 6709-17.

Maniere, G., Alves, G., Berthelot-Grosjean, M. and Grosjean, Y. (2020). Growth regulation by amino acid transporters in Drosophila larvae. *Cell Mol Life Sci* **77**, 4289-4297.

Marygold, S. J., Roote, J., Reuter, G., Lambertsson, A., Ashburner, M., Millburn, G. H., Harrison, P. M., Yu, Z., Kenmochi, N., Kaufman, T. C. et al. (2007). The ribosomal protein genes and Minute loci of Drosophila melanogaster. *Genome Biol* **8**, R216.

McCarthy, R. L., Kaeding, K. E., Keller, S. H., Zhong, Y., Xu, L., Hsieh, A., Hou, Y., Donahue, G., Becker, J. S., Alberto, O. et al. (2021). Diverse heterochromatin-associated proteins repress distinct classes of genes and repetitive elements. *Nat Cell Biol* **23**, 905-914.

Milkereit, P., Gadal, O., Podtelejnikov, A., Trumtel, S., Gas, N., Petfalski, E., Tollervey, D., Mann, M., Hurt, E. and Tschochner, H. (2001). Maturation and intranuclear transport of pre-ribosomes requires Noc proteins. *Cell* **105**, 499-509.

Mills, E. W. and Green, R. (2017). Ribosomopathies: There's strength in numbers. *Science* **358**.

Narla, A. and Ebert, B. L. (2010). Ribosomopathies: human disorders of ribosome dysfunction. *Blood* **115**, 3196-205.

Neumuller, R. A., Gross, T., Samsonova, A. A., Vinayagam, A., Buckner, M., Founk, K., Hu, Y., Sharifpoor, S., Rosebrock, A. P., Andrews, B. et al. (2013). Conserved regulators of nucleolar size revealed by global phenotypic analyses. *Sci Signal* **6**, ra70.

Nijhout, H. F., Riddiford, L. M., Mirth, C., Shingleton, A. W., Suzuki, Y. and Callier, V. (2014). The developmental control of size in insects. *Wiley Interdiscip Rev Dev Biol* **3**, 113-34.

Palm, W., Sampaio, J. L., Brankatschk, M., Carvalho, M., Mahmoud, A., Shevchenko, A. and Eaton, S. (2012). Lipoproteins in Drosophila melanogaster--assembly, function, and influence on tissue lipid composition. *PLoS Genet* **8**, e1002828.

Parisi, F., Riccardo, S., Daniel, M., Saqcena, M., Kundu, N., Pession, A., Grifoni, D., Stocker, H., Tabak, E. and Bellosta, P. (2011). Drosophila insulin and target of rapamycin (TOR) pathways regulate GSK3 beta activity to control Myc stability and determine Myc expression in vivo. *BMC Biol* **9**, 65.

Parisi, F., Riccardo, S., Zola, S., Lora, C., Grifoni, D., Brown, L. M. and Bellosta, P. (2013). dMyc expression in the fat body affects DILP2 release and increases the expression of the fat desaturase Desat1 resulting in organismal growth. *Dev Biol* **379**, 64-75.

Penzo, M., Montanaro, L., Trere, D. and Derenzini, M. (2019). The Ribosome Biogenesis-Cancer Connection. *Cells* **8**.

Pirillo, A., Casula, M., Olmastroni, E., Norata, G. D. and Catapano, A. L. (2021). Global epidemiology of dyslipidaemias. *Nat Rev Cardiol*.

Port, F., Strein, C., Stricker, M., Rauscher, B., Heigwer, F., Zhou, J., Beyersdorffer, C., Frei, J., Hess, A., Kern, K. et al. (2020). A large-scale resource for tissue-specific CRISPR mutagenesis in Drosophila. *Elife* **9**.

Quin, J. E., Devlin, J. R., Cameron, D., Hannan, K. M., Pearson, R. B. and Hannan, R. D. (2014). Targeting the nucleolus for cancer intervention. *Biochim Biophys Acta* **1842**, 802-16.

Rusten, T. E., Lindmo, K., Juhasz, G., Sass, M., Seglen, P. O., Brech, A. and Stenmark, H. (2004). Programmed autophagy in the Drosophila fat body is induced by ecdysone through regulation of the PI3K pathway. *Dev Cell* **7**, 179-92.

Saeboe-Larssen, S., Lyamouri, M., Merriam, J., Oksvold, M. P. and Lambertsson, A. (1998). Ribosomal protein insufficiency and the minute syndrome in Drosophila: a dose-response relationship. *Genetics* **148**, 1215-24.

Saeboe-Larssen, S., Urbanczyk Mohebi, B. and Lambertsson, A. (1997). The Drosophila ribosomal protein L14-encoding gene, identified by a novel Minute mutation in a dense cluster of previously undescribed genes in cytogenetic region 66D. *Mol Gen Genet* **255**, 141-51.

Sanchez, J. A., Mesquita, D., Ingaramo, M. C., Ariel, F., Milan, M. and Dekanty, A. (2019). Eiger/TNFalpha-mediated Dilp8 and ROS production coordinate intra-organ growth in Drosophila. *PLoS Genet* **15**, e1008133.

Schmid, M. R., Anderl, I., Vesala, L., Vanha-aho, L. M., Deng, X. J., Ramet, M. and Hultmark, D. (2014). Control of Drosophila blood cell activation via Toll signaling in the fat body. *PLoS One* **9**, e102568.

Scott, R. C., Schuldiner, O. and Neufeld, T. P. (2004). Role and regulation of starvation-induced autophagy in the Drosophila fat body. *Dev Cell* **7**, 167-78.

Shokri, L., Inukai, S., Hafner, A., Weinand, K., Hens, K., Vedenko, A., Gisselbrecht, S. S., Dainese, R., Bischof, J., Furger, E. et al. (2019). A Comprehensive Drosophila melanogaster Transcription Factor Interactome. *Cell Rep* **27**, 955-970 e7.

Texada, M. J., Koyama, T. and Rewitz, K. (2020). Regulation of Body Size and Growth Control. *Genetics* **216**, 269-313.

Tortoriello, G., de Celis, J. F. and Furia, M. (2010). Linking pseudouridine synthases to growth, development and cell competition. *FEBS J* **277**, 3249-63.

Valenza, A., Bonfanti, C., Pasini, M. E. and Bellosta, P. (2018). Anthocyanins Function as Anti-Inflammatory Agents in a Drosophila Model for Adipose Tissue Macrophage Infiltration. *Biomed Res Int* **2018**, 6413172.

Vallejo, D. M., Juarez-Carreno, S., Bolivar, J., Morante, J. and Dominguez, M. (2015). A brain circuit that synchronizes growth and maturation revealed through Dilp8 binding to Lgr3. *Science* **350**, aac6767.

van Riggelen, J., Yetil, A. and Felsher, D. W. (2010). MYC as a regulator of ribosome biogenesis and protein synthesis. *Nat Rev Cancer* **10**, 301-9.

Figures and Table

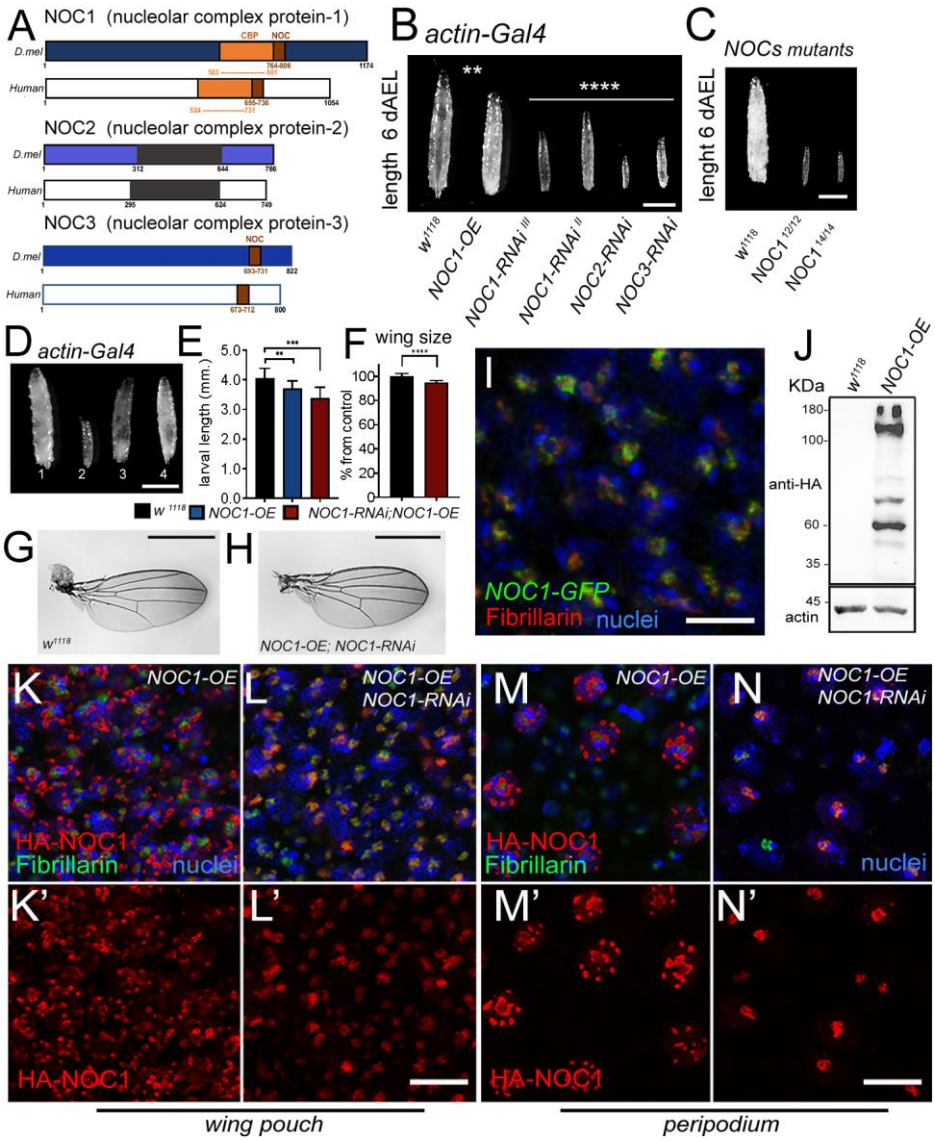

Fig. 1. NOC1 is expressed in the nucleolus and its reduction, like for NOC2 and NOC3, affects animal growth and survival. (A) Schematic representation of *Drosophila* NOC1, NOC2 and NOC3 proteins and their human homologues. NOC1 protein contains a CBP domain (CCAAT binding domain), in orange, that shares 32% identity between sequences. In brown is represented the conserved NOC domain of 45 amino acids, present only in NOC1 and NOC3, that share 48% and 38% sequence identity between *D.mel* and human proteins respectively. NOC2 protein shares an overall 36% identity between *D.mel* and human proteins; in black is represented the region of highest homology (48%). (B) Photos of third instar larvae expressing the indicated transgenes under the *actin* driver, taken at 120 hours after egg laying (AEL); the scale bar represents 1 mm. (C) Photos of control and

NOC1^{12} and *NOC1*^{14} mutant third instar larvae of 120 hours AEL; scale bar 1mm. (D) Photographs of larvae at 120 hours AEL expressing the following transgenes (1) control *w*^{1118}, (2) *NOC1-RNAi*, (3) *NOC1* overexpression (OE), (4) *NOC1-RNAi; NOC1-OE* using the *actin-Gal4* driver; scale bar 1mm. (E) Larval length measured in mm at 120 hours AEL. (F) Quantification of the wing's area/size in animals of the indicated genotype; the number is expressed as % from the control *actin-w*^{1118}, the error bars indicate the standard deviations. At least 10 animals were used for each genotype, experiment was repeated twice. (G-H) Photos representing wings from females of the indicated genotypes; the scale bars in G and H represent 1 mm. (I) Confocal image of cells from the wing imaginal disc showing *NOC1-GFP* expression visualized using anti-GFP antibodies in green, and anti-fibrillarin in red; nuclei are visualized with Hoechst; scale bar represents 5 μm. (J) Western blot from larval lysates expressing *HA-NOC1* under the *actin* promoter. A band of about 130 KDa is the expected size for NOC1, is visualized by anti-HA antibody with few other bands at lower molecular weight; actin is used as control loading. (K-N) Confocal pictures of cells from the wing imaginal discs (K-L) or from the peripodial epithelium (M-N) expressing *HA-NOC1* (K-M) or *HA-NOC1;NOC1-RNAi* (L-N) using the *engrailed*-promoter. NOC1 expression was visualized using anti-HA antibodies in red and anti-fibrillarin in green. Statistical analysis in E was calculated using one-way ANOVA with Tukey multi-comparisons test from at least 10 animals ** = $p < 0.01$, *** = $p < 0.001$ and **** = $p < 0.0001$, and the error bars indicate the standard deviations. Statistical analysis in F was calculated using Student's *t*-test from at least 10 animals ** = $p < 0.01$, *** = $p < 0.001$ and **** = $p < 0.0001$, and the error bars indicate the standard deviations.

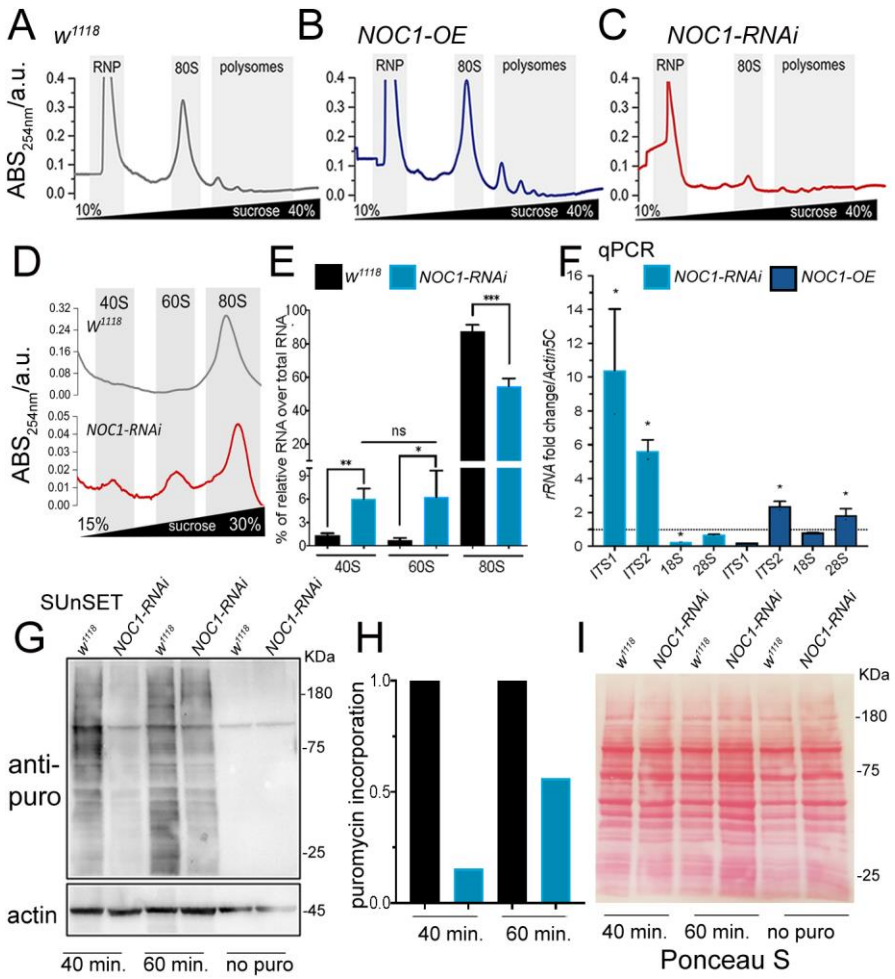

Fig. 2. NOC1 regulates rRNA processing and ribosomal assembling, affecting protein synthesis. (A-C) Representative sucrose density gradient profiles of ribosome from control larvae (A) or animals over-expressing *NOC1* (B) or *NOC1-RNAi* (C). (D) Higher resolution of image A and C highlighting the area of the 40, 60 and 80S ribosomal subunits, note that the graphs use different scales. (E) Analysis of the % of 40, 60 and 80S ribosomal subunits, relative to each genotype, calculated over the total area including the polysome. (F) qRT-PCR showing the fold of induction over control w^{1118} of pre-rRNAs analyzed using the ITSs (internal transcribed sequences) and of mature ribosomal rRNAs; data are expressed over *actin5C* used as control. (G) SUnSET western blot analysis of lysates from larvae treated with puromycin for the indicated time. The blot shows the relative changes in protein synthesis using anti-puromycin antibodies in control w^{1118} or in larvae ubiquitously expressing *NOC1-RNAi* under the *actin*-promoter. Actin was used as control loading. (H) Quantification of the change in puromycin incorporation from G and normalized over actin (Deliu et al., 2017). (I) Ponceau S staining showing total

protein levels in G. Statistical analysis in E and F was calculated using one-way ANOVA with Tukey multi-comparisons test from at least three independent experiments * = $p < 0.05$ ** = $p < 0.01$ and *** = $p < 0.001$; the error bars indicate the standard deviations.

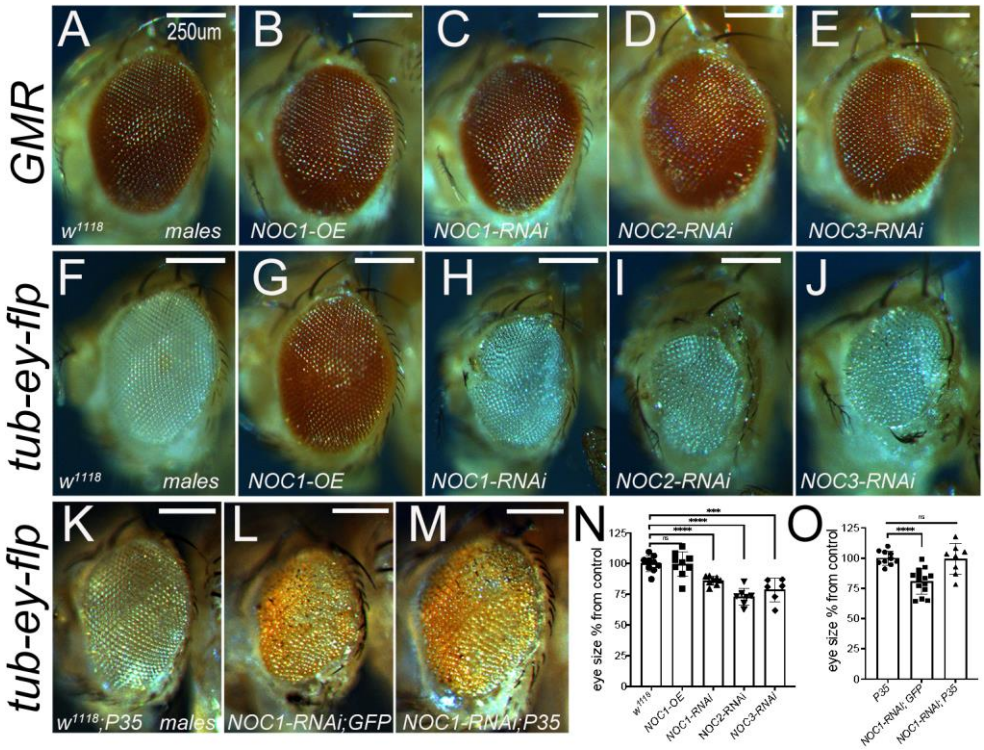

Fig. 3. Reduction of NOC1, NOC2 and NOC3 during development affects the number and size of the ommatidia by inducing apoptosis but does not affect the differentiated ommatidia. Photographs of *Drosophila* compound eyes (lateral view) expressing the indicated transgenes using the *GMR-Gal4* promoter (A-E) or the *tubulin-GAl4* promoter in combination with *eyeless-flippase* to constrain Gal4 expression in the proliferative cells of the eye and antenna (F-J) (Bellosta et al., 2005). (K-M) Photographs of compound eyes expressing the caspase inhibitor *P35* alone (K) or together with *NOC1-RNAi* (M) that rescues the eye defect showed in L. The scale bars represent 250 μm. Photographs were acquired from male's eyes and similar data were obtained using females (not shown). (N) Quantification of eye size from F-J (O) and from K-M experiments; values are expressed as % from the control. Statistical analysis in N and O was calculated using Student's *t*-test from at number of animals indicated *** = $p < 0.001$ and ****= $p < 0.0001$; the error bars indicate the standard deviations.

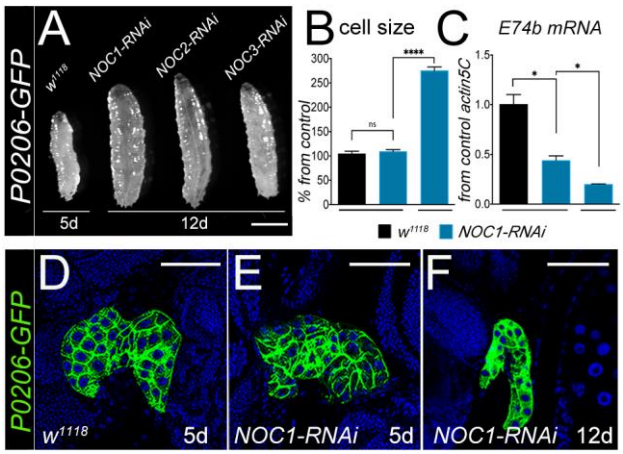

Fig. 4. NOC1 downregulation in the prothoracic gland (PG) reduces ecdysone production and delays development. (A) Photographs of whole animals with reduced NOCs expression in the prothoracic gland, driven by the *P0206* promoter. Picture represents w^{1118} larvae at 5 days AEL and *NOC1-RNAi, NOC2-RNAi and NOC3-RNAi* at 12 days AEL. The scale bar represents 1 mm. (B) Analysis of the size in cells of the fat body from control w^{1118} or *NOC1-RNAi* larvae at 5 days and at 12 days AEL. (C) qRT-PCR showing the level of *E74b* mRNA, target of ecdysone, from whole larvae at the indicated time of development. (D-F) Confocal images of the ring gland marked with GFP, using the *P0206-GFP* driver line, from control w^{1118} (D) and from animals with reduced *NOC1* at 5 days AEL (E) and 12 days AEL (F). Nuclei are stained with Hoechst; the scale bars represents 50 μm. Statistical analysis in B and C was calculated using one-way ANOVA with Tukey multi-comparisons test from at least two independent experiments, more than 10 animals were used in each experiment * = $p < 0.05$ and **** = $p < 0.0001$; the error bars indicate the standard deviations.

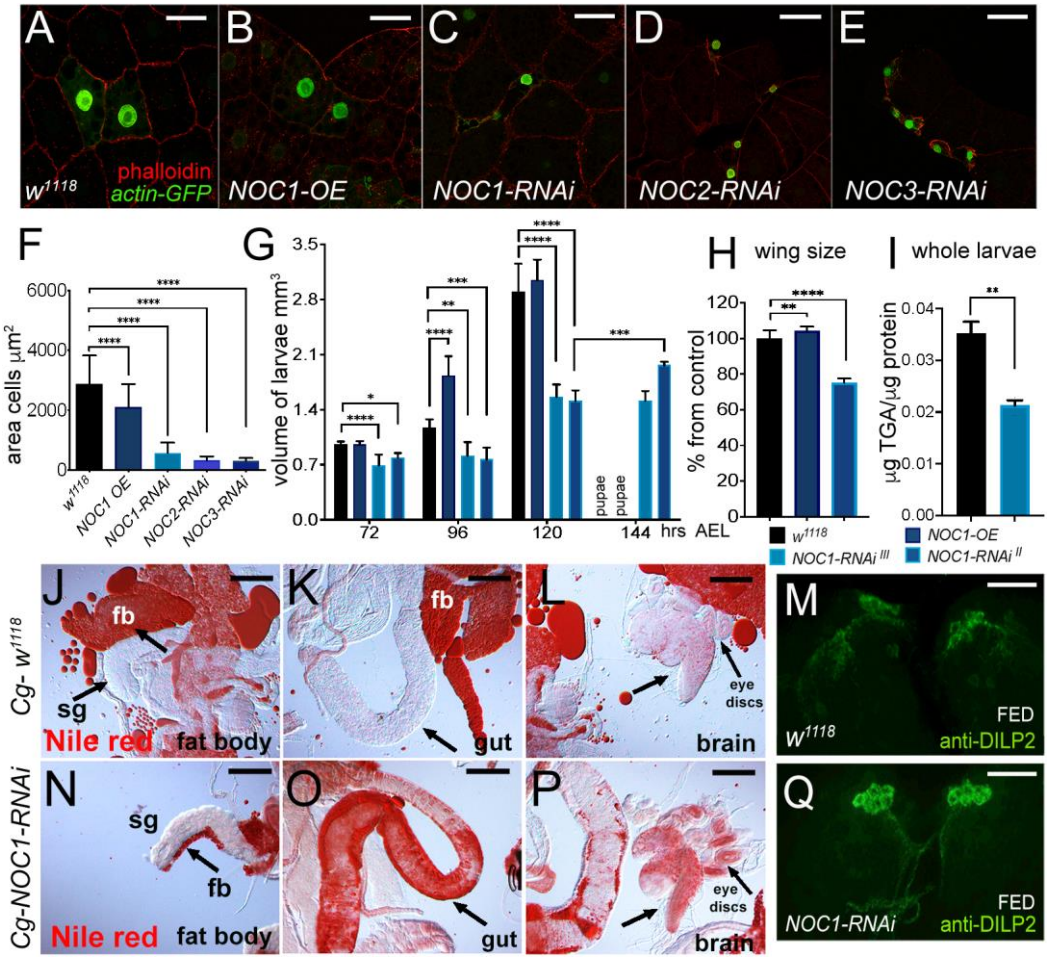

Fig. 5. NOC1 downregulation in the fat body reduces its size and TAGs contents resulting in larval lethality and induces dyslipidemia. (A-E) Confocal images of *actin*-flip-out clones in the fat body co-expressing nuclear GFP together with the indicated transgenes. Phalloidin-Texas Red was used to mark cell membranes; the scale bars represent 50 µm. (F) Quantification of the size of the cells in the clones from the fat body. (G) Analysis of larval volume measured at the indicated time of development until pupariation in animals in which the NOCs transgenes were expressed using the *Cg* promoter. (H) Analysis of the wing size from four days old females of the indicated genotypes, data are expressed as % from control w^{1118}. (I) Quantification of triglycerides (TGAs) in whole larvae at 120 hours AEL, data are expressed as µg of TGAs/µg of proteins. (J-L, N-P) Photographs of larval organs stained with Nile red to visualized lipids from control w^{1118} (J-L) and NOC1-RNAi animals (N-P) at third instar. (J-N) Reduction of *NOC1-RNAi* affects the size of the fat body (fb) particularly visible near the salivary gland (sg indicated by the arrow); the scale bar represents 100 µm. The impairment to

accumulate nutrients in the fat body in *NOC1-RNAi* animals induces the storage of fats in other organs, visible in the gut indicated by the arrow in K and O, and in the brain and eye imaginal discs, indicated by the arrow in L and P. (M, Q) Confocal images of third instar larval brains showing DILP2 immunostaining in the Insulin Producing Cells (IPCs) from control w^{1118} (M) and *NOC1-RNAi* (Q) animals in feeding conditions; the scale bar represents 50 μm. Data in G are representative of one of three experiments using ten or more animals for each genotype; data in F, G and H were calculated using one-way ANOVA with Tukey multi-comparisons test from at least two independent experiments; data in I were calculated using Student's *t* test from two independent experiments; * = $p < 0.05$, ** = $p < 0.01$, *** = $p < 0.001$and **** = $p < 0.0001$, the error bars indicate the standard deviations.

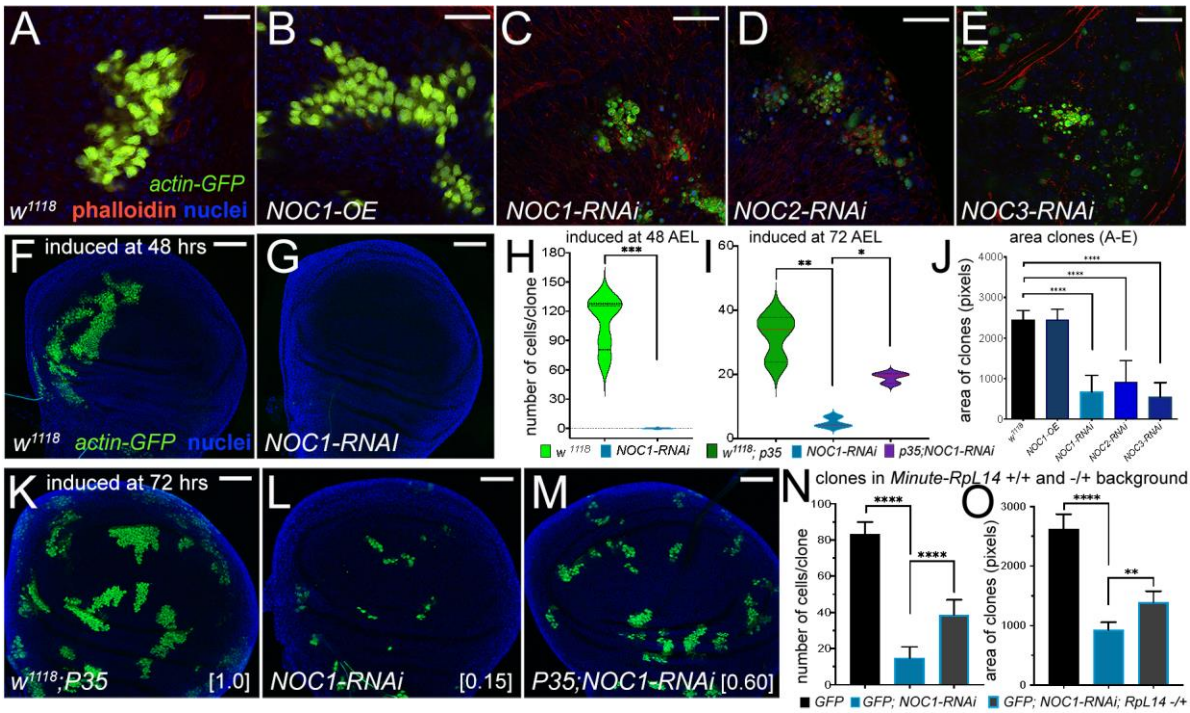

Fig. 6. Reduction of NOC1, NOC2 and NOC3 in cells of the wing imaginal disc induces growth defects that are rescued by co-expressing P35 and in a *Minute (3)66D*/+ heterozygous background. (A-E) Confocal images of *actin*-flip-out clones analyzed in the wing imaginal discs, expressing nuclear GFP and the indicated transgenes. Phalloidin-Texas Red was used to mark the cell membranes (red) and Hoechst for the nuclei (blue). (J) Quantification of clonal size was performed by measuring the area marked by phalloidin; area is shown in pixels. At least 15 animals from each genotype were used; the scale bar represents 20 μm. (F, G) Confocal images of wing imaginal discs showing *actin*-flip-out clones expressing GFP alone (F) or co-expressing *NOC1-RNAi* (G). Clones were induced at 48 hours AEL; the scale bar represents 50 μm. (H-I) Quantification of the number of cells in each clone was analyzed at 120 hours AEL using GFP as marker. (K-M) Photographs of *actin*-flip-out clones in wing discs expressing GFP along with the inhibitor of caspase P35 (K), or with *NOC1-RNAi* (L) or co-expressing *NOC1-RNAi* together with P35 (M); clones were induced at 72 hours AEL. The number of cells in each clone from K, L and M was quantified at 120 hours AEL. The total number of clones analyzed in this experiment is indicated in parenthesis: w^{1118} + P35 (72), *NOC1-RNAi* alone (66), and *NOC1-RNAi* + p35 (81). The numbers in square brackets represent the relative size of clones (average) compared to that from

control considered equal to 1. (N-O) Analysis cell number and clonal size of *NOC1-RNAi* clones induced in Rp+/- a Rp+/+ background using the *Minute(3)66D/+* line that carries a mutation in the Rpl14 protein. (N) Quantification of the number of clones in each disc. (O) Clonal size showing that defects of *NOC1-RNAi* cells are partially rescued when clones are grown in the *Minute(3)66D/+* (Rp-/+) background. Data in H were calculated using Student's *t* test. The asterisks in the graphs in I, J, N and O represent the *p*-values from one-way analysis of variance (ANOVA) with Tukey multiple comparisons * = $p < 0.05$, ** = $p < 0.01$, *** = $p < 0.001$ and **** = $p < 0.0001$, and the error bars indicate the standard deviations. In figures F, G, K-M, Hoechst was used for staining the nuclei.

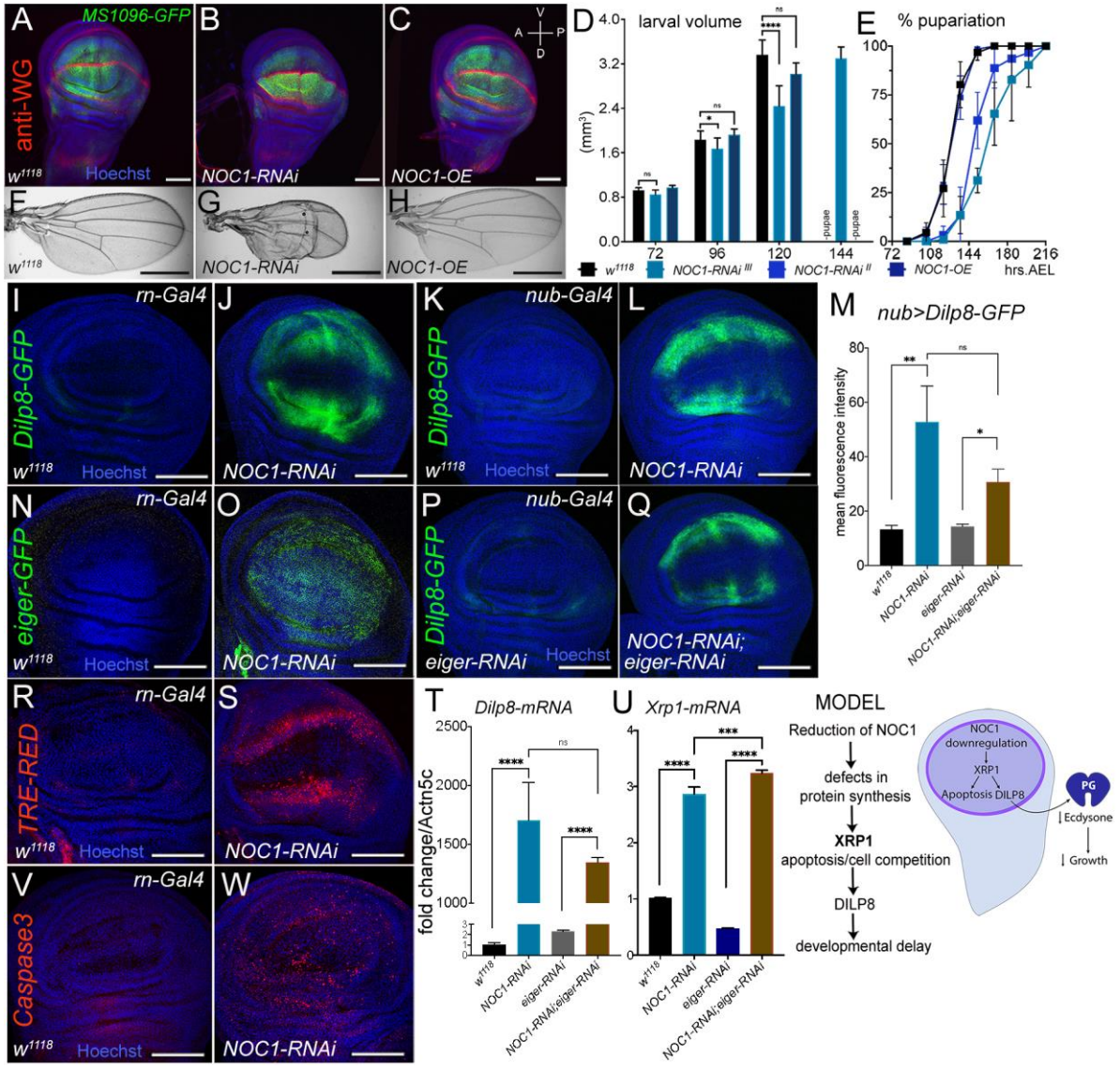

Fig. 7. Reduction of NOC1 in cells of the wing imaginal disc induces Xrp1 and eiger resulting in apoptosis and DILP8-induced developmental delay. (A-C) Confocal images of wing imaginal discs expressing the indicated transgenes using the *MS1096-GFP* wing-driver. Wingless (WG) expression is visualized using anti-WG antibodies (in red), nuclei are stained with Hoechst (in blue); the scale bar represents 40 μm. (D) Larval volume of animals expressing the indicated transgenes using the *MS1096*-driver was measured at the indicated time after egg laying (AEL) until pupariation. The graph is representative of one of three experiments using at least ten animals for each point and genotype, the asterisks represent the *p*-values from one-way (ANOVA) with Tukey multiple comparisons * = $p < 0.05$, ** = $p < 0.01$, *** = $p < 0.001$and **** = $p < 0.0001$, the error bars indicate the standard deviations. (E) Curves representing the % of pupariation of animals at the indicated genotypes.

A significant delay in pupariation (one-way ANOVA, $p < 0,0001$) is visible in animals in which *NOC1* is reduced using *MS1096-Gal4* with both the RNAi lines. Data are expressed as % of pupariation over the total number of pupae of the same genotype, and the error bars indicate the standard deviations from five independent experiments. (F-H) Photographs of wings from three days old adults of the indicated genotype; the scale bar represents 1 mm. (I-W) Confocal images of wing imaginal discs from third instar larvae where *NOC1-RNAi* was expressed using *rotund-Gal4* driver co-expressing *DILP8-GFP* (I-J), *eiger-GFP* (N-O), TRE-dsRED (R-S) reporters, or stained for apoptotic cells using anti-Caspase-3 antibody (V-W); (K-Q) Confocal images of wing imaginal discs expressing *NOC1-RNAi* using the *nubbin-Gal4* driver (K-L) or together with *eiger-RNAi* (P-Q), along with the *DILP8-GFP* reporter. The scale bars represent 100 μm. (M) Quantification of the mean of GFP intensity in the wing pouch from K, L, O, P. (T-U) qRT-PCRs showing the level of *DILP8* (T) and *Xrp1* (U) mRNAs in wing imaginal discs in which NOC1 and eiger levels were reduced using the *rotund-Gal4* promoter; *actin5C mRNA* was used as control. MODEL: NOC1 is necessary for proper rRNA processing. Its reduction decreases protein synthesis and induces a nucleolar stress resulting in apoptosis. This event is accompanied by the upregulation of the pro-apoptotic genes *eiger* and Xrp1, resulting in DILP8 upregulation that in turn reduces ecdysone delaying animal development.

Table 1. Characterization of NOCs expression *in vivo* using different promoters

Promoter		transgene	larval stage	pupal stage	adult
whole body	*actin* [1]	NOC1 OE	vital	lethal	-
		NOC1-RNAi	lethal at L2, small	-	-
		NOC2-RNAi	lethal at L2, small	-	-
		NOC3-RNAi	lethal at L2, small	-	-
		NOC1RNAi NOC1 OE	vital, small size [2]	vital	vital, small size
neurons	*elav*	NOC1 OE	vital	vital	vital, no eye defects
		NOC1-RNAi	delayed	lethal	-
		NOC2-RNAi	delayed	lethal	-
		NOC3-RNAi	delayed	lethal	-
retina	*GMR* [3]	NOC1-RNAi	vital	vital	vital, no eye defect
		NOC1-RNAi	vital	vital	vital, no eye defects
		NOC2-RNAi	vital	vital	vital, no eye defects
		NOC3-RNAi	vital	vital	vital, no eye defects
eye-ant	*tub-ey>flp* [4]	NOC1 OE	vital	vital	vital, no eye defects
		NOC1-RNAi	vital	vital	vital, small eye, defects
		NOC2-RNAi	vital	vital	vital, small eye, defects
		NOC3-RNAi	vital	vital	vital, small eye, defects
PG	*P0206* [5]	NOC1 OE	vital	vital	vital, no defects
		NOC1-RNAi	delayed, big larvae	no pupae	-
		NOC2-RNAi	delayed, big larvae	no pupae	-
		NOC3-RNAi	delayed, big larvae	no pupae	-
fat body	*Cg* [6]	NOC1 OE	vital	vital	increased body size
		NOC1-RNAi	delayed, semi lethal at L3	semi lethal, small	lethal, few escapers *
		NOC2-RNAi	delayed, lethal at L2/L3	lethal, small pupae	-
		NOC3-RNAi	delayed, lethal at L2/L3	lethal, small pupae	-
	FB [6]	NOC1 OE	vital	vital	vital, body size (ND)
		NOC1-RNAi	delayed, lethal at L3	small pupae, lethal	-
		NOC2-RNAi	delayed, lethal at L3	small pupae, lethal	-
		NOC3-RNAi	delayed, lethal at L3	small pupae, lethal	-
wing	*MS1096* [7]	NOC1 OE	vital	vital	vital **
		NOC1-RNAi	delayed	vital	vital, crumpled wings
		NOC2-RNAi	delayed	vital	vital, crumpled wings
		NOC3-RNAi	delayed	vital	vital, crumpled wings
	engrailed [8]	NOC1 OE	vital	vital	vital
		NOC1-RNAi	delayed, lethal ***	-	-
		NOC2-RNAi	delayed, lethal	-	-
		NOC3-RNAi	delayed, lethal	-	-
		NOC1-RNAi NOC1 OE	vital, rescue	vital	vital

[1-2] see Figure 1B, D. [3] see Figure 3A-E. [4] see Figure 3F-J. [5] see Figure 4A. [6] see Figure 5G, H, * few escapers are born with small body size using line on Chromosome II. [7] see Figure 7D, E, ** few males are born with wing defects being *MS1096* in on Chromosome X. [8] see Supplementary Figure 3, *** immature imaginal discs are visible in NOC1-RNAi larvae using a transgene on Chromosome II, while fewer imaginal discs are found using the RNAi line on Chromosome III.

(A)

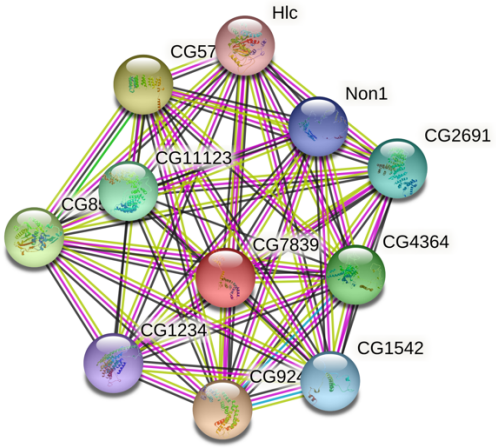

(B)

Your Input:

		Neighborhood	Gene Fusion	Cooccurence	Coexpression	Experiments	Databases	Textmining	[Homology]	Score
CG7839	IP14658p; Sequence-specific DNA binding transcription factor activity. It is involved in the biological process described with: regulation of transcription, DNA-templated; neurogenesis (1174 aa)									

Predicted Functional Partners:

CG9246	Nucleolar complex protein 2 homolog; It is involved in the biological process described with: neurogenesis				●	●		●		0.997
CG5728	LD41803p; mRNA binding. It is involved in the biological process described with: regulation of alternative mRNA splicing, via ...				●	●		●		0.995
CG8545	LD11307p; RNA binding; S-adenosylmethionine-dependent methyltransferase activity. It is involved in the biological process d...				●	●		○		0.995
CG4364	Pescadillo homolog; Required for maturation of ribosomal RNAs and formation of the large ribosomal subunit				●	●		●		0.988
CG11123	RH42110p; RNA binding				●	○		●		0.984
CG2691	RRP12-like protein; It is involved in the biological process described with: neuron projection morphogenesis				●	●		●		0.982
CG1542	Probable rRNA-processing protein EBP2 homolog; Required for the processing of the 27S pre-rRNA				●	●		●		0.982
Non1	Nucleolar GTP-binding protein 1; Involved in the biogenesis of the 60S ribosomal subunit (By similarity). Required for normal ...				●	●		●		0.982
CG1234	annotation not available				●	○		●		0.981
Hlc	Helicase, isoform A; ATP binding; ATP-dependent RNA helicase activity; nucleic acid binding. It is involved in the biological pr...				●	●		○		0.979

Fig. S1. Protein-protein interaction network generated using STRING (Szklarczyk et al., 2019)

(A) Graphic representation and (B) predicted list of the functional partners of NOC1/CG7839, members of the interaction network.

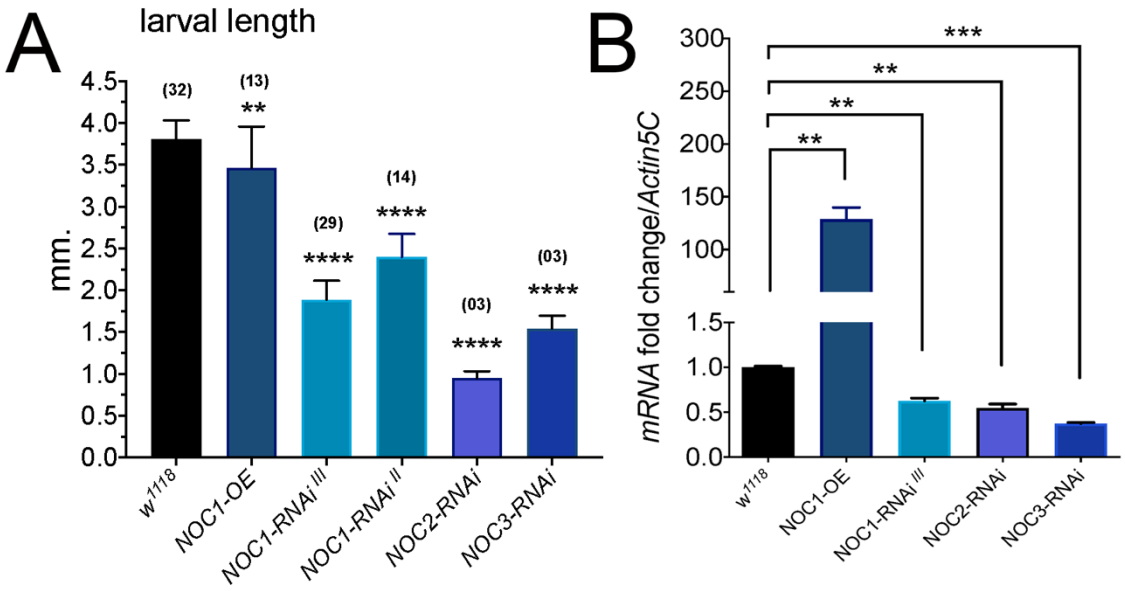

Fig. S2A-B. Length of larvae (A) and the relative mRNA expression (B) in whole larvae overexpressing *NOC1* or with downregulation of *NOC1, 2* and *3* using the *actin-Gal4* promoter.

(A) Larval Length was measured at 120 hours AEL. The asterisks represent the *p*-values from one-way analysis of variance (ANOVA) with Tukey multiple comparisons ** = $p < 0.01$ and **** = $p < 0.0001$, and the error bars indicate the standard deviations for each genotype. In parenthesis is indicated the number of animals analyzed. (B) qRT-PCR showing the relative amount of *NOCs mRNA* upon RNA overexpression or interference. *NOC1-OE* and *NOCs-RNAi* were ubiquitously expressed using the *actin-Gal4* promoter. RNA was extracted from whole larvae. *p*-values were calculated from Student's *t*-test from at least two independent experiments: ** = $p < 0.01$, *** = $p < 0.001$ and **** = $p < 0.0001$, the error bars indicate the standard deviations.

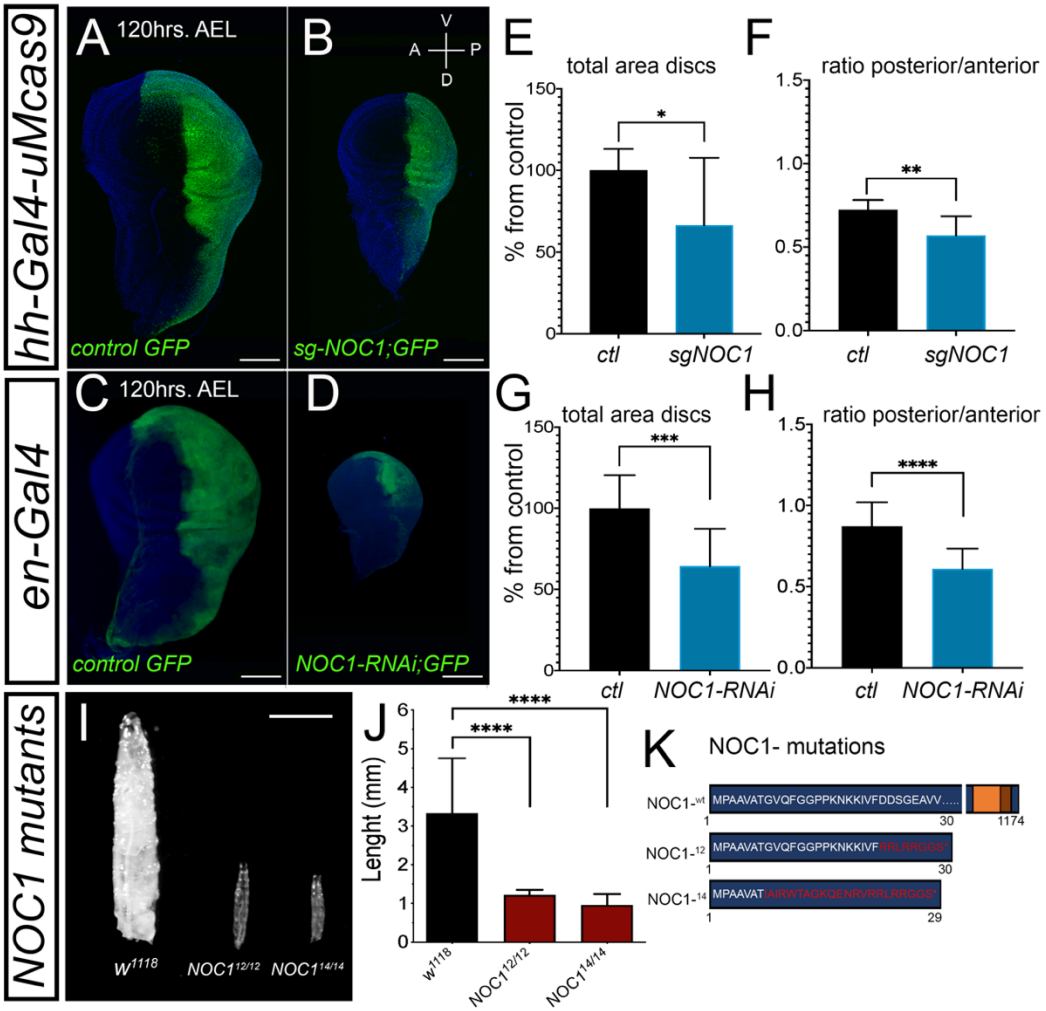

Fig. S3. NOC1 CRISPR mutation affects animal growth and phenocopies NOC1 downregulation induced by RNA interference in the wing disc.

To develop genomic *NOC1* mutants, we induced site specific mutations with the CRISPR-Cas9 system, using the line *sgRNA*^{CG7839} from Boutros's laboratory (Port et al., 2020). To analyze if the reduction of NOC1 with this system phenocopied the data with *engrailed*-Gal4, we used a line that carries the *hedgehog-Gal4* to drive *UAS-Cas9* to express *sgRNA*^{CG7839} in the posterior compartment of the wing disc. As shown in Figure A-B, driving mutations of NOC1 using *hedgehog-Gal4* compromised and reduced the development of the posterior compartment of the wing disc within a similar extent to that observed with *engrailed-NOC1-RNAi* (C-D). To compare the efficiency of the two systems, we analyzed the total area of imaginal discs and the ratio between the area of the posterior compartment (marked by co-expression of GFP) and the anterior from animals at 120 hours AEL. This analysis showed that reduction of NOC1 using *sgRNA*^{CG7839} affected the total area of the discs and the ratio between the posterior and the anterior compartments (E-F). These data resembled that obtained using NOC1-RNAi expressed under the *engrailed* promoter (G-H). To introduce NOC1 mutations in the germ line, we used the *nos-Gal4, UAS-Cas9* line crossed with *sgRNA*^{CG7839}. Sequencing analysis of 30 NOC1 heterozygous lines revealed the presence of missense mutations in the NOC1 gene in two lines, which encoded for very short polypeptides of 30 and 29 amino acids in length in *NOC1-mut12* and *NOC1-mut14*, respectively (K). Moreover, the phenotypic analysis of these two homozygous NOC1 mutants showed a robust growth defect at the larval stage (I and J, also shown in Figure 1C), recapitulating the phenotype described in the *actin-NOC1-RNAi* larvae (Figure 1B).

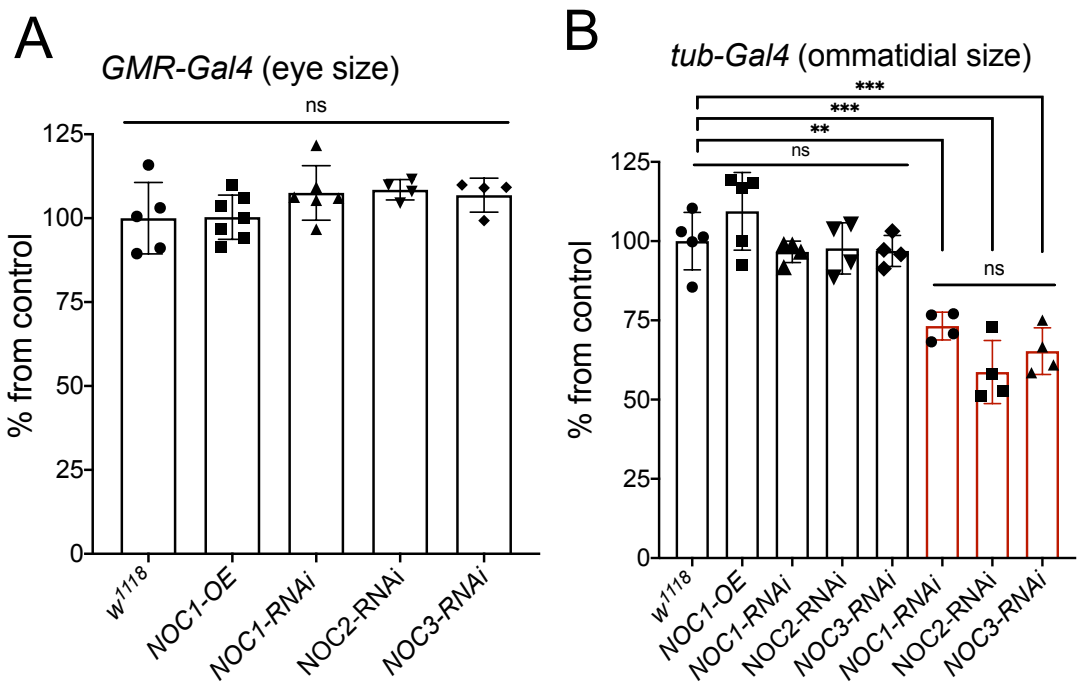

Fig. S4. (A) Quantification of the eye size from animals expressing the indicated transgenes using the *GMR-Gal4* promoter, (B) or the ommatidial size using the *tubulin-Gal4* promoter. Values are expressed as % from the control. Statistical analysis was calculated using Student's *t*-test from the number of animals indicated in the experiment. The error bars indicate the standard deviations.

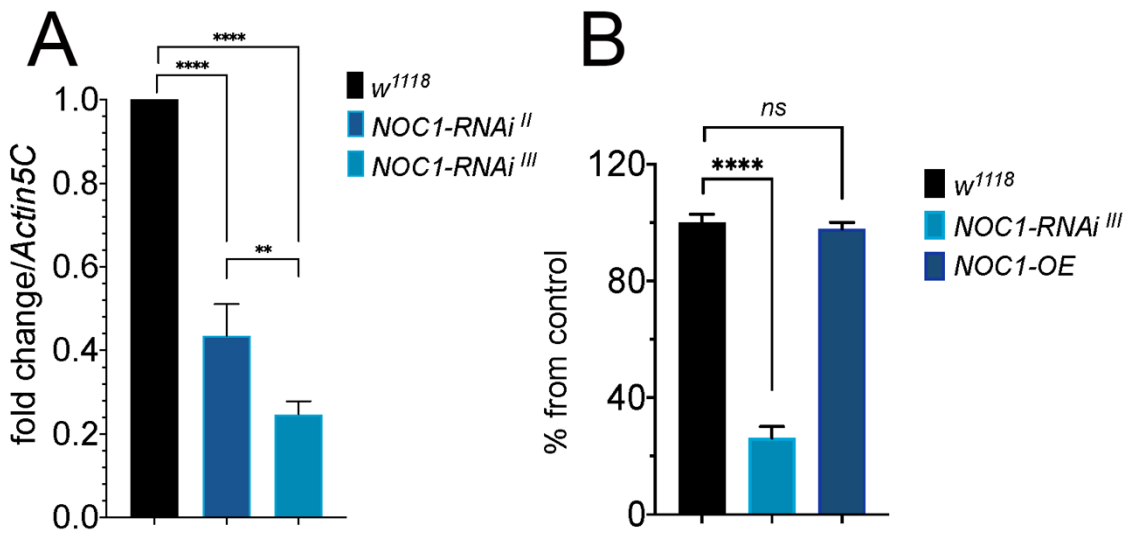

Fig. S5 A-B. (A) qRT-PCR showing the relative amount of *NOC1 mRNA* upon expression of the indicated transgenes using the ubiquitous *actin-Gal4* promoter. RNA was extracted from whole larvae. *p*-values were calculated from Student's *t*-test from at least two independent experiments: ** = $p < 0.01$, **** = $p < 0.0001$, the error bars indicate the standard deviations. **(B) Analysis of the size of wings in adult females of the indicated genotypes.** *p*-values were calculated from Student's *t*-test from at least two independent experiments: * = $p < 0.05$, ** = $p < 0.01$, **** = $p < 0.0001$, the error bars indicate the standard deviations. At least 10 animals were used for w^{1118} and *NOC1-OE*, while for *NOC1-RNAi*$^{-II}$ only 4 were born as adults (escapers).

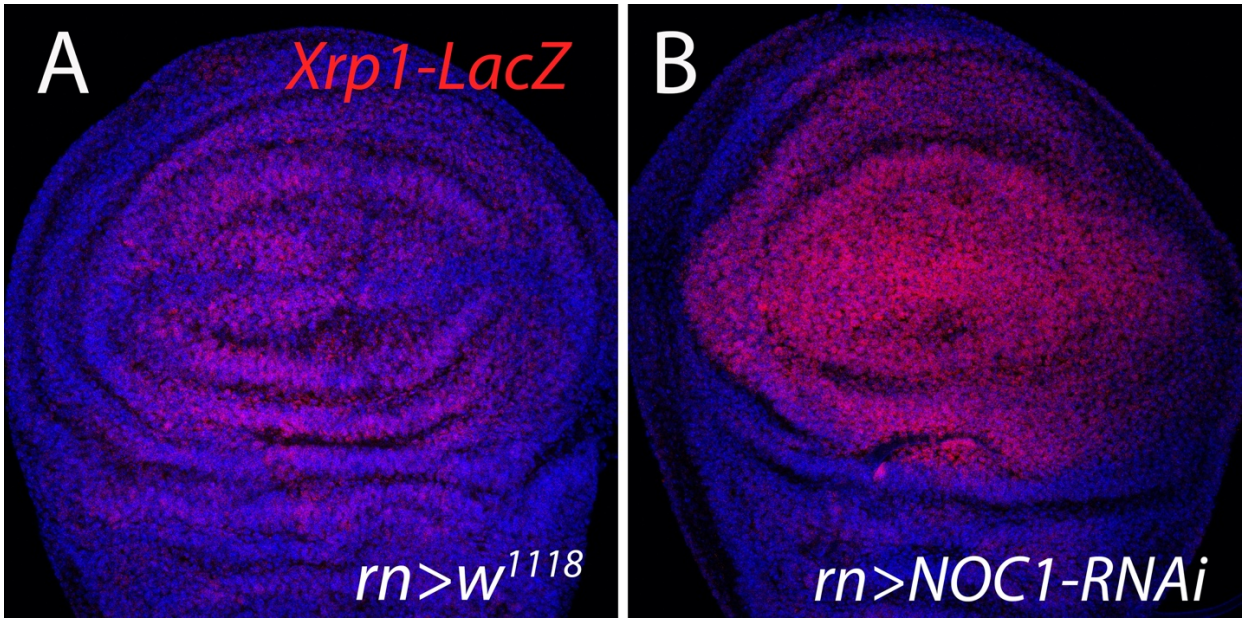

Fig. S6. Confocal images of wing imaginal discs showing increased activation of Xrp1 promoter upon expression of NOC1-RNAi using the *rotund-Gal4* promoter. *NOC1-RNAi* was expressed using the *rn-Gal4* promoter in a line carrying the $Xrp1^{02515}$-lacZ as a reporter for the activation of XRP1 (Baillon et al., 2018). Third instar imaginal discs were dissected and analyzed for LacZ expression using anti-beta gal antibody (red). Nuclei were stained with Hoechst (blue). $w^{1118}Xrp1^{02515}$ was used as control.

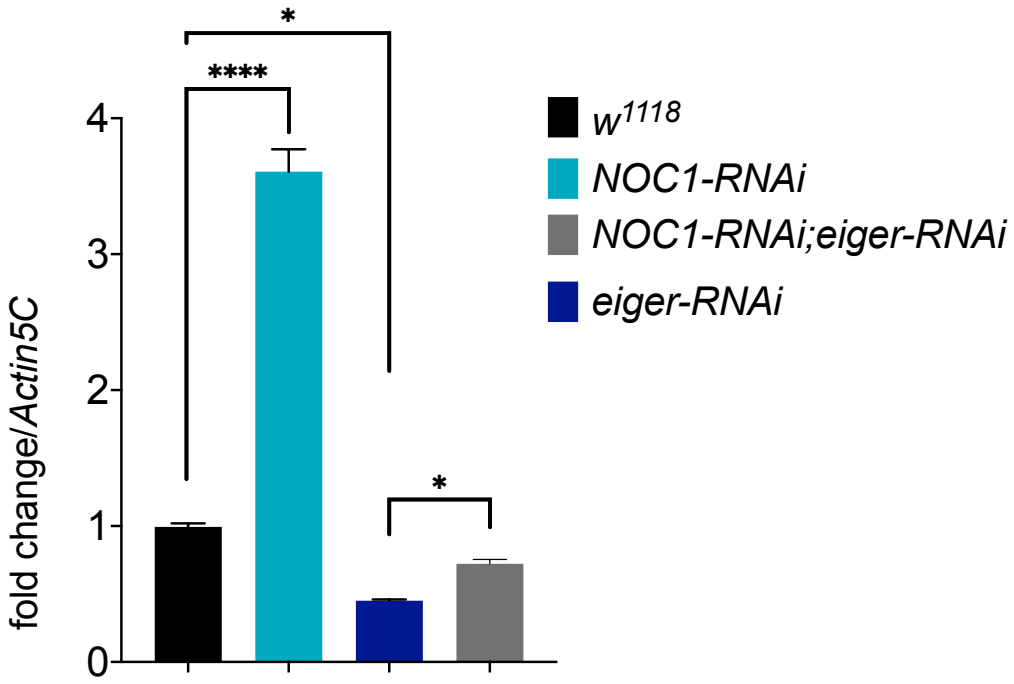

Fig. S7. qRT-PCR showing the relative amount of *eiger-mRNA* in wing imaginal discs from animals of the indicated genotypes. *NOC1-RNAi* or in combination with *eiger-RNAi* were expressed using the *nubbin-Gal4* promoter. RNA was extracted from imaginal discs. *p*-values were calculated with One-way ANOVA * = $p < 0.05$, **** = $p < 0.0001$, the error bars indicate the standard deviations.

Table S1. Selected list of potential targets of CEBPz involved in ribosomal biogenesis and nucleolar control. Data are from TCGA datasets from cBio Cancer Genomic Portal from Liver Hepatocellular Carcinoma (A) and Breast Cancer (B). *common proteins

A

liver tumor	p Value
DKC1/NOP60b	6.71E-15
FBL	0.000001171
NOP10	0.00007354
NOP16	0.000008451
NOP2*	1.59E-10
NOP56	0.000001243
NOP58	5.18E-14
RPS7*	5.54E-12
RPS16	0.0008972
RPS18	0.005751
RPS20	0.0000206
RPS21	0.0007177
RPS27A	1.23E-08
RPS2P32	0.0000032
RPSA	0.004546
RPL5	0.0005937
RPL7	0.0191
RPL21	0.0005989
RPL24*	0.00188
RPL30	0.00006775
RPL35A*	0.0001787
RPL38	0.0008094
RPL39	0.00004626

B

brast tumor	p Value
NOP2*	0.0454
RPS7*	3.36E-04
RPS8	0.0325
RPL5	0.0444
RPL12	0.0225
RPL14	0.0389
RPL24*	0.0333
RPL27	0.032
RPL32	0.047
RPL35	0.044
RPL35A*	0.0419

Table S2. List of PRIMERS used for qRT-PCRs

gene	5' FW sequence	5' REV sequence	reference
NOC1	CTATACGCTCCACCGCACAT	GTCGCTACCGAACTTGTCCA	this work
NOC2	AGGAGCTTGAAGGGCTTAAAGA	ATCCTTGCTGGGTTTGTGGTA	this work
NOC3	TGCAGGCAGGCAAAAATCAC	AGCAAGCGTTTCATGAAGGC	this work
E74b	GAATCCGTAGCCTCCGACTGT	AGGAGGGAGAGTGGTGGTGTT	(Colombani et al., 2005)
Actin5c	CAGATCATGTTCGAGACCTTCAAC	ACGACCGGAGGCGTACAG	(Colombani et al., 2005)
Dilp8	CGACAGAAG GTCCATCGAGT	GTT TTGCCG GATCCAAGTC	(Boulan et al., 2019)
NOC1 genomic	GTCACGGTCATTTCAATGGTA	CATGTCCAGCACCTCATC	this work
ITS1	GAAGAAACAAAATTCGAAAG	CGTATGCCCATAACTAAGAT	Neumuller et al., 2013)
ITS2	ATCTTAGTTATGGGCATACG	CTGGCATATATCAATTCCTT	(Neumuller et al., 201
18S	CTCATATCCGAGGCCCTGTA	ACGAACGTTTTAACCGCAAC	(Neumuller et al., 2013)
28S	CGCTACGTCCGTTGGATTAT	CAATGCAAATTGCCCCTTAT	(Neumuller et al., 2013)
XRP1	GACCACACCGGAGATTATCAA	GCTGGTACTGGTACTTGTGGTG	(Baillon et al., 2018)
Eiger	AAAGGTGGATGGCCTCACG	TGCCGGTATGTGCATTGTTG	this work

Baillon, L., Germani, F., Rockel, C., Hilchenbach, J. and Basler, K. (2018). Xrp1 is a transcription factor required for cell competition-driven elimination of loser cells. *Sci Rep* **8**, 17712.

Boulan, L., Andersen, D., Colombani, J., Boone, E. and Leopold, P. (2019). Inter-Organ Growth Coordination Is Mediated by the Xrp1-Dilp8 Axis in Drosophila. *Dev Cell* **49**, 811-818 e4.

Colombani, J., Bianchini, L., Layalle, S., Pondeville, E., Dauphin-Villemant, C., Antoniewski, C., Carre, C., Noselli, S. and Leopold, P. (2005). Antagonistic actions of ecdysone and insulins determine final size in Drosophila. *Science* **310**, 667-70.

Neumuller, R. A., Gross, T., Samsonova, A. A., Vinayagam, A., Buckner, M., Founk, K., Hu, Y., Sharifpoor, S., Rosebrock, A. P., Andrews, B. et al. (2013). Conserved regulators of nucleolar size revealed by global phenotypic analyses. *Sci Signal* **6**, ra70.

Port, F., Strein, C., Stricker, M., Rauscher, B., Heigwer, F., Zhou, J., Beyersdorffer, C., Frei, J., Hess, A., Kern, K. et al. (2020). A large-scale resource for tissue-specific CRISPR mutagenesis in Drosophila. *Elife* **9**.

Szklarczyk, D., Gable, A. L., Lyon, D., Junge, A., Wyder, S., Huerta-Cepas, J., Simonovic, M., Doncheva, N. T., Morris, J. H., Bork, P. et al. (2019). STRING v11: protein-protein association networks with increased coverage, supporting functional discovery in genome-wide experimental datasets. *Nucleic Acids Res* **47**, D607-D613.